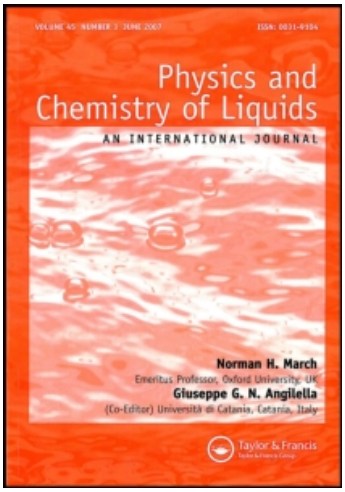

Physics and Chemistry of Liquids
Publication details, including instructions for authors and subscription information:
http://www.informaworld.com/smpp/title~content=t713646857

Phase Stability Analysis in Binary Systems

Hugo Segura[a]; Ilya Polishuk[b]; Jaime Wisniak[b]
[a] Group of Surface Characterization and Statistical Thermodynamics, Department of Chemical Engineering, Universidad de Concepción, Concepción, Chile [b] Department of Chemical Engineering, Ben-Gurion University of the Negev, Beer-Sheva, Israel

To cite this Article Segura, Hugo , Polishuk, Ilya and Wisniak, Jaime(2000) 'Phase Stability Analysis in Binary Systems', Physics and Chemistry of Liquids, 38: 3, 277 — 331
To link to this Article: DOI: 10.1080/00319100008030279
URL: http://dx.doi.org/10.1080/00319100008030279

Phys. Chem. Liq., 2000, Vol. 38, pp. 277–331
Reprints available directly from the publisher
Photocopying permitted by license only

PHASE STABILITY ANALYSIS IN BINARY SYSTEMS

HUGO SEGURA[a,*], ILYA POLISHUK[b] and JAIME WISNIAK[b]

[a] *Group of Surface Characterization and Statistical Thermodynamics, Department of Chemical Engineering, Universidad de Concepción, POB 53-C, Concepción, Chile;*
[b] *Department of Chemical Engineering, Ben-Gurion University of the Negev, Beer-Sheva 84105, Israel*

(Received 9 November 1998)

Stability analysis should be a standard practice for testing the *physical validity* of phase equilibrium states predicted by thermodynamic models however, it is seldom used in routine work of experimental data modeling. Lack of stability analysis may result in potential modeling pitfalls or in an inadequate prediction of data. In this contribution the concept of stability is reviewed from a general viewpoint, showing how it applies to completely general cases of binary phase equilibrium, from low to high-pressure ranges. Graphical examples are given using excess Gibbs energy models and equations of state.

Keywords: Stability; phase equilibrium; tangent plane criterion; critical lines

INTRODUCTION

The design, simulation and optimization of equilibrium separation processes depend on the availability of phase *equilibrium* data and appropriate *models* used for correlation purposes. Experimental data must fulfill various requirements, particularly consistency (or data reliability) and availability in a wide temperature and pressure ranges. In addition to a proper fit of reliable data, the adequacy of models depends on their predictive capabilities, for which stability analysis plays a central role. In fact, stability analysis should be a standard practice

*Corresponding author. e-mail: hsegura@diq.udec.cl

for testing the *physical validity* of phase equilibrium states predicted or correlated using thermodynamic models. Excess Gibbs energy (G^E) models in the $\gamma-\phi$ approach to phase-equilibrium, or equations of state (EOS) in the $\phi-\phi$ approach, are intended for the reduction of experimental equilibrium data that represent global stability in well carried-out experiments. Although it is common practice to perform stability analysis in the treatment of liquid–liquid equilibrium (LLE) data [1] and in multiphase flash equilibrium predictions, it is not always so when correlating low-pressure phase equilibrium. This may result in potential pitfalls in the analysis of vapor–liquid equilibrium (VLE) data, as discussed by Wisniak *et al.* [2], or in solid–liquid equilibrium (SLE) data correlation, as pointed out by Marcilla *et al.* [3]. Testing for stability is strongly recommended also in quasi-critical equilibrium calculations, where multiphase equilibrium may be observed as a consequence of the topology of critical lines [4]. However, it is seldom done when correlating supercritical fluid extraction (SFE) data by means of EOS.

The theoretical basis of thermodynamic stability was first stated by Gibbs: a homogeneous phase with a given composition is stable when its Gibbs energy is minimum at constant temperature and pressure. This requirement implies, as *a necessary condition*, that the matrix of the second derivatives of the Gibbs energy with respect to the independent compositions be positive definite, and originates from the theory of local extreme points [5]. From a mathematical viewpoint, the condition given by Gibbs is achieved when the Gibbs energy function of a system yields *relative and absolute* minima; both types of stationary points establish equilibrium states and are physically permissible, but define two different classes of stability:

- *Intrinsic stability*, which implies that at constant temperature and pressure the Gibbs energy of a system is minimum, *although not necessarily an absolute minimum*,
- *Global stability*, which implies that at constant temperature and pressure the Gibbs energy of a system is *an absolute minimum*. Note that a global stable state satisfies intrinsic stability, which is a *necessary but not sufficient condition* of global stability.

The difference between intrinsic and global stability lies on the stability of a given equilibrium state, where a minimum of the Gibbs

energy has been achieved, with respect to small or large perturbations. In order to clarify these concepts it is instructive to consider the mechanical analog of the Gibbs energy shown in Figure 1 where the spontaneous evolution of a thermodynamic system to an equilibrium state is analyzed. Curve ABCDE represents a possible trajectory of the system (represented by a ball) to an equilibrium state. Points B and D represent positions where the system will remain at rest, spontaneously (as required for equilibrium). Any other position implies dynamic evolution to lower energy states. Let us now consider the equilibrium states B and D. If the system in state B is subject to a small perturbation and then allowed to evolve to an equilibrium state, it is very probable that it will return to the original state B. However, if it is subjected to large perturbations, large enough to overcame the energetic barrier BC, the system will evolve to point D which is a point of absolute minimum energy. Point B represents a position of *metastable*

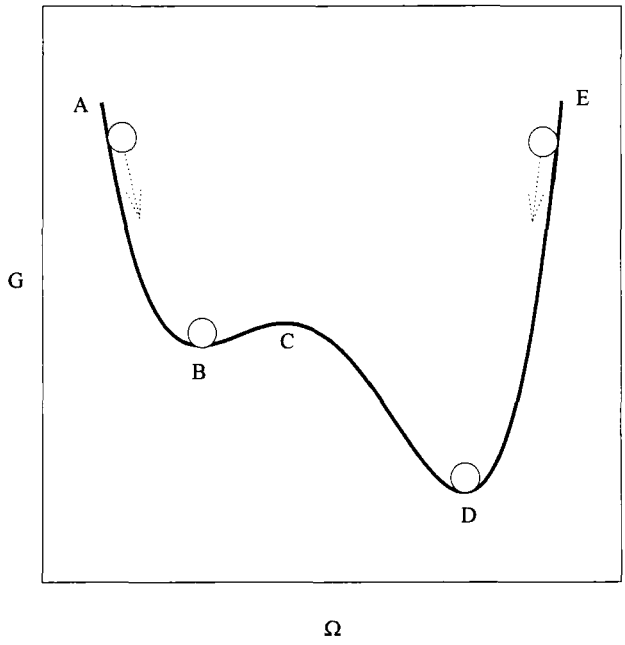

FIGURE 1 Mechanical analog for the stability of a system and its equilibrium states. Ω represents the allowable states of the system at constant temperature, pressure and total mass.

equilibrium that may be broken by large perturbations and D represents a position of *absolute* equilibrium. The Gibbs energy may be considered as *the potential energy* of a thermodynamic system, and from this analogy it follows that global stable equilibrium states, or states of absolute minimum Gibbs energy, are *hierarchically* dominant over those states which yield relative minima of the Gibbs energy. Metastability may be observed experimentally, the barrier that stabilizes these states corresponds to the energy required for the nucleation of embryo phases once saturation conditions have been achieved [6]. Examples of these situations are the release of vapor bubbles from a saturated liquid phase and the generation of liquid drops during condensation. The design of experimental equipment and techniques should be intended to avoid metastability in phase equilibrium measurements, the objective being the experimental determination of global stable data. In fact, global stability is *assumed* (without verification) in almost every equilibrium data published.

The models used for correlation purposes must reflect also the global stability of experimental data. From a modeling viewpoint, although intrinsic stability may be predicted for a homogeneous phase (or for a phase equilibrium state), the possibility of predicting equilibrium states that are more stable (*i.e.*, states which may yield lower Gibbs energy values), like VLE, LLE, or SLE, demands further testing to determine if a predicted equilibrium state represents a global minimum of the *total* Gibbs energy.

Intrinsic and global stability differences were early recognized by the van der Waals school [7] when predicting gas–liquid and liquid–liquid critical lines with the van der Waals equation. In critical equilibrium calculations the limit of intrinsic stability is always achieved along a critical line because the conditions for calculating the critical point contains this requirement. Nevertheless, the curve branches of calculated critical lines do not yield necessarily global stability, and may originate critical end points between fluid phases (as discussed by Van Konyenburg and Scott [4], or between solid and fluid phases [8]). End points constraint the global stability of critical equilibrium states, a common case being heteroazeotropy which limits the existence of a critical LLE line, because pressure (or temperature) allows the stabilization of a vapor phase, thus interrupting the continuity of critical LL immiscibility at lower pressures (or higher temperatures).

As we have seen so far, stability analysis is directly related to a Gibbs energy minimization problem which, in turn, may be expressed in terms of thermodynamic models, at constant temperature and pressure. Every minimum of the Gibbs energy corresponds to an equilibrium state, *but only the lowest value* defines the most stable or the globally stable state of a system that is of interest for phase equilibrium predictions. The proper methodology for establishing unequivocally a global minimum of energy is *the tangent plane* criterion discussed by Baker *et al.* [9], because it meets global stability conditions and assures the necessary and sufficient conditions for an overall minimum of the Gibbs energy in the *whole* composition range. Nowadays, it is possible to utilize well-established methods based on the tangent plane criterion for performing global stability analysis together with routine equilibrium data treatment [10–12]. The tangent plane criterion allows a simple geometrical interpretation but its numerical implementation is complex and continues to be a challenge for sophisticated minimization algorithms, particularly when considering the general case of multicomponent heterogeneous phase equilibrium. The main difficulty, which remains for a robust numerical implementation of the tangent plane criterion, lies on the complex mathematical nature of the problem. For example, the Gibbs energy surface may be sectionally differentiable in multiphase equilibrium (it can be also a noncontinuous function for particular phases), so common differential techniques for continuous functions cannot be applied directly. Also, in multiphase equilibrium, the Gibbs energy surface is a highly non-linear function of the composition and can exhibit a set of multiple minima, difficulting the precise localization of the absolute one. In spite of these difficulties, common cases of binary phase equilibrium allow a simple graphical solution of the problem using the Gibbs energy of mixing diagram, a technique that should be an obvious candidate for stability analysis. As pointed out by Radzyminski and Whiting [13], the general case of heterogeneous equilibrium between fluid phases of different density does not correspond to the typical Gibbs energy diagrams which are usually presented in many textbooks to illustrate the tangent plane criterion. This fact is particularly significant when considering a graphical stability analysis for binary mixtures using an EOS of the van der Waals type (or those derived from perturbation theories, as discussed by Reed and Gubbins [14]), or when using the $\gamma-\phi$ approach.

In this contribution the basic concepts of stability are reviewed and the work of Radzyminski and Whiting [13] is extended to stability analysis of multiphase binary equilibrium, yielding simple and straightforward rules which can be applied for a critical assessment of data correlation and prediction. Examples are provided to illustrate the different situations discussed.

THEORY

Let us start our analysis of the problem by considering a simple closed system that is differentially perturbed by the transfer of small amounts of energy in the form of work and/or heat. We will consider the evolution of the system once the energetic perturbations are stopped; state in which the system will *spontaneously* achieve equilibrium. The evolution to an equilibrium state can be studied using two independent principles of conservation: the energy balance and the entropy balances

$$dU = \delta Q + \delta W \tag{1}$$

$$dS = \frac{\delta Q}{T} + dS_{\text{gen}} \tag{2}$$

In Eq. (2) the term S_{gen} represents the entropy generation and will always be positive, as required by the Second Law of thermodynamics. Replacing in Eq. (1) yields

$$dU = TdS - TdS_{\text{gen}} + \delta W \tag{3}$$

For quasi-static perturbations the mechanical work is given by $\delta W = -PdV$ where P is the pressure of the system. Replacing in Eq. (3), taking into account the sign of entropy generation, yields

$$dU - TdS + PdV = -TdS_{\text{gen}} \leq 0 \tag{4}$$

When a system reaches a state of equilibrium the generation term (which depends on gradients of pressure, temperature, and chemical potential) becomes zero and Eq. (4) yields

$$dU - TdS + PdV \underbrace{=}_{\substack{\text{equilibrium} \\ \text{state}}} 0 \tag{5}$$

At constant temperature and pressure Eq. (4) becomes:

$$d(U - TS + PV)_{T,P} \leq 0 \tag{6}$$

By definition the sum $U - TS + PV = G$, the Gibbs energy G of a closed system, hence, at constant temperature and pressure, an isolated system will evolve to an equilibrium state when the following differential constant is fulfilled

$$dG_{T,P} \leq 0 \tag{7a}$$

Equilibrium conditions will be met when

$$dG_{T,P} = 0 \tag{7b}$$

According to Eqs. (7) the spontaneous evolution to equilibrium of a closed is indicated by a reduction of its Gibbs energy. Since the temperature and the pressure remain constant during the equilibration process, the evolution to equilibrium conditions is caused by nonzero chemical potential gradients. In addition, Eq. (7b) establishes that for an equilibrium state the Gibbs energy reaches an stationary point (*maximum or minimum*), for which Eq. (7a) imposes an additional constraint that is met when the equilibrium state corresponds to a *local* minimum of the Gibbs energy. Equations (7) constitute the *necessary* and *sufficient conditions* of an equilibrium state, which are not necessarily a phase equilibrium condition but a homogeneous state where pressure, temperature and chemical potential gradients become zero for the whole system. The concept of stability is related to the specific case of phase equilibrium because of the inability of the system to exist as a homogeneous phase or, equivalently, due to the fact that the Gibbs energy is not a minimum for a homogeneous phase but for heterogeneous phase equilibrium. Hence, analysis of the stability of a homogeneous phase constitutes also an assessment of the possibility of a phase-equilibrium state. Equations (7) are useful for studying the stability analysis of a system that is constrained to differential perturbations and they constitute the definition of intrinsic stability.

Integration of Eq. (7a) yields

$$\Delta G_{T,P} \leq 0 \tag{8}$$

According to Eq. (8), in every spontaneous change of a system at constant temperature and pressure, the observed overall change of the Gibbs energy must be negative. Equation (8) also constitutes a *stability criteria* because it constraints the possible evolution path of a system towards an equilibrium state. However, according to Eq. (8), the scale of the perturbation is arbitrary and not necessarily differential, so that Eq. (8) may be applied also for assessing the global stability of a system.

Let us consider now the mixing process of two pure fluids at constant temperature and pressure, as shown in Figure 2. For this process the Gibbs energy of mixing, ΔG, is given by

$$\Delta G = G - \sum_{i}^{N} n_i \, \tilde{G}_i \tag{9}$$

where G is the total Gibbs energy of the mixture and $\tilde{G}_i$ is the Gibbs energy of the pure component, all evaluated at the same temperature and pressure. On a molar basis

$$\Delta \tilde{G} = \tilde{G} - \sum_{i}^{N} x_i \, \tilde{G}_i \leq 0 \tag{10}$$

In terms of partial properties the Gibbs energy of a mixture is given by:

$$\tilde{G} = \sum_{i}^{N} x_i \, \overline{G}_i = \sum_{i}^{N} x_i \mu_i \tag{11}$$

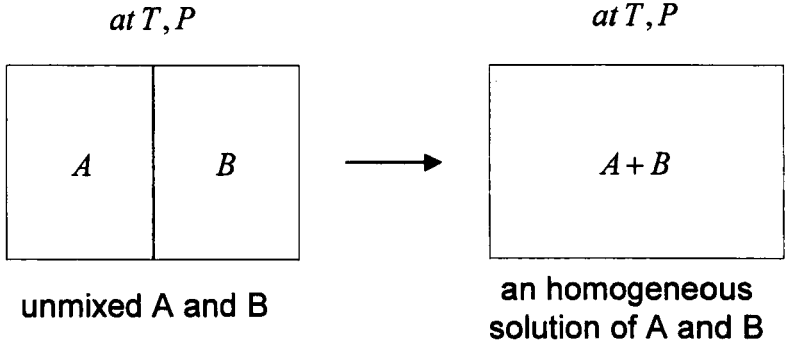

FIGURE 2 A mixing process.

where μ_i is the chemical potential and $\overline{G}_i$ is the partial Gibbs energy. Combining Eqs. (10) and (11) yields:

$$\Delta\widetilde{G} = \sum_{i}^{N} x_i(\overline{G}_i - \widetilde{G}_i) \leq 0 \tag{12}$$

The constraint given by Eq. (12) expresses the principle of spontaneity: mixing of fluids is possible only when the Gibbs energy of mixing is negative, otherwise, the pure fluids will remain immiscible and no homogeneous mixture will be possible.

According to our previous arguments, Eq. (12) constitutes a constraint to the stability of a mixture in a homogeneous phase and, as will be shown below, it has the advantage of being readily expressible in terms of thermodynamic models. Figures 3 to 5 illustrate typical situations that may be obtained for Eq. (12) when analyzing a mixture

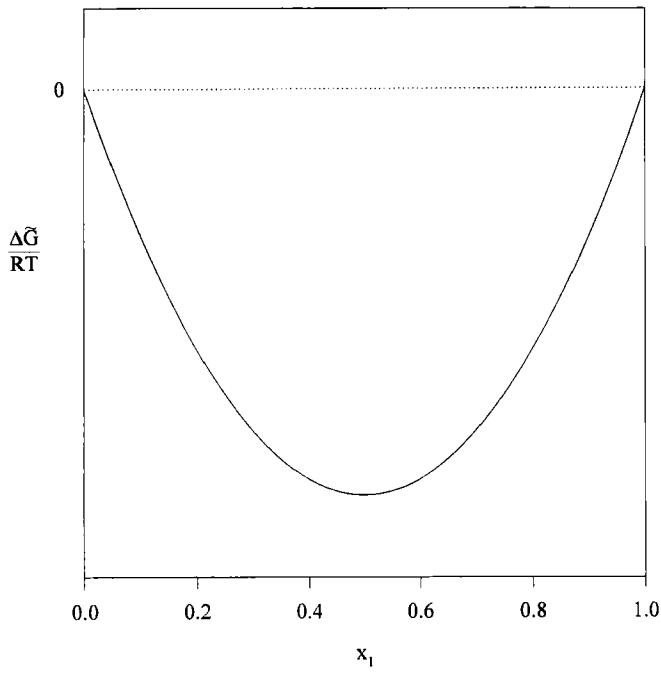

FIGURE 3 Completely miscible system.

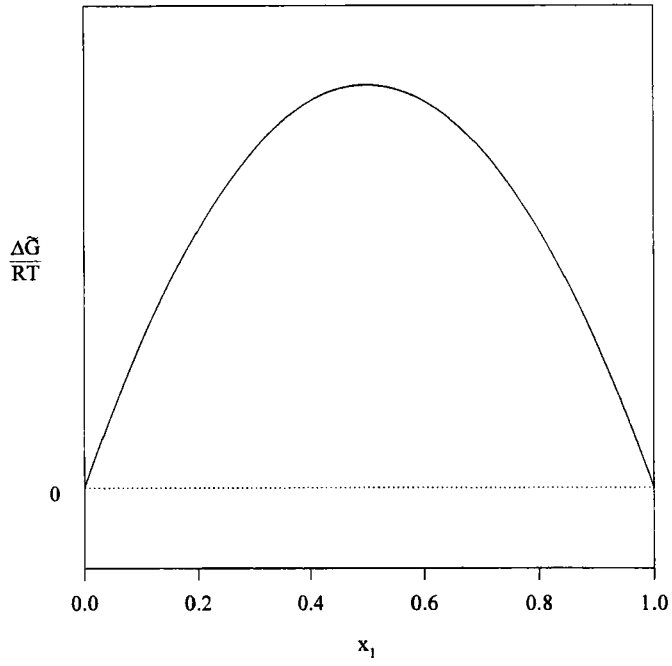

FIGURE 4 Absolute immiscible system.

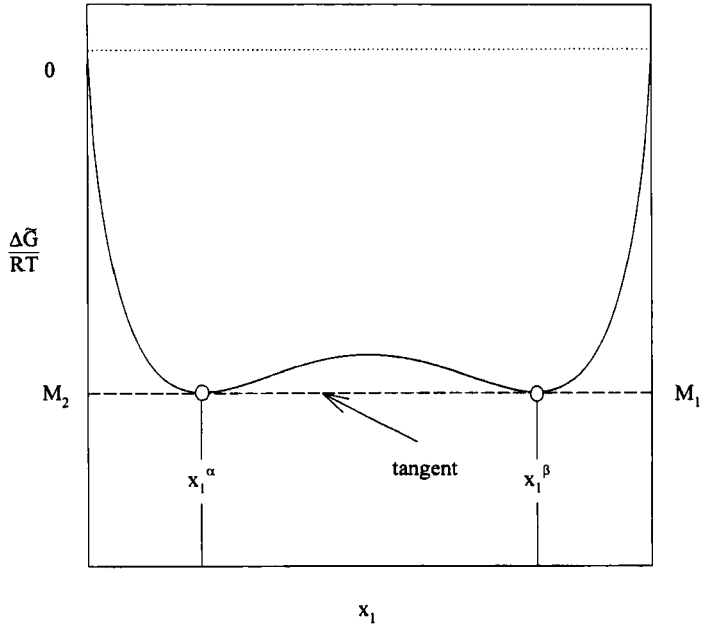

FIGURE 5 Partially miscible system.

in a single-phase state. An example is a liquid mixture whose possible states may be plotted by a unique $\Delta\widetilde{G}$ curve (this will not be so when considering more general cases where phases in different states, for example liquid and vapor, satisfy phase equilibrium conditions). Some composition ranges of the curves under consideration (to be indicated by dotted lines) may be experimentally inaccessible but, nevertheless, *may be predicted* by models. Figure 3 illustrates a case of complete miscibility, for every composition a negative value of the mixing Gibbs energy is achieved, indicating that the mixture is a homogeneous phase or, in other words, the homogeneous phase is stable for every possible concentration. Figure 4 represents a case of complete immiscibility, every concentration yields a positive value of $\Delta\widetilde{G}/RT$, indicating that the mixing process is impossible because it violates the stability constraint given by Eq. (12). In this particular case two phases are present, each corresponding to a pure component. Figure 5 represents a case of partial miscibility, in spite the fact that negative $\Delta\widetilde{G}/RT$ values are observed for the full composition range and hence, deserves further analysis. Inspection of Figure 5 reveals that the $\Delta\widetilde{G}/RT$ function has two inflection points and that the concavity of the $\Delta\widetilde{G}/RT$ function changes with the composition, at constant temperature and pressure. Let us now analyze the particular tangent M_1-M_2 shown in the figure, this tangent touches the $\Delta\widetilde{G}/RT$ curve at the two compositions x_1^α and x_1^β. For these two compositions the common tangent intercepts at $x_1 = 0$ and $x_1 = 1$ are:

$$\begin{aligned} M_1(x_1^\alpha) &= M_1(x_1^\beta) \\ M_2(x_1^\alpha) &= M_2(x_1^\beta) \end{aligned} \tag{13}$$

These intercepts are related to the partial mixing Gibbs energies and to the chemical potentials as follow [15]

$$M_i = \frac{\Delta\overline{G}_i}{RT} = \frac{\mu_i - \mu_i^*}{RT} \tag{14}$$

In Eq. (14) μ_i^* is the chemical potential of the pure component at the same temperature and pressure of the mixture. Combining with

Eqs. (13) and (14) gives

$$M_1(x_1^\alpha) = M_1(x_1^\beta) \Rightarrow \frac{\Delta\overline{G}_1(x_1^\alpha)}{RT} = \frac{\Delta\overline{G}_1(x_1^\beta)}{RT} \Rightarrow \mu_1(x_1^\alpha) = \mu_1(x_1^\beta)$$
$$M_2(x_1^\alpha) = M_2(x_1^\beta) \Rightarrow \frac{\Delta\overline{G}_2(x_1^\alpha)}{RT} = \frac{\Delta\overline{G}_2(x_1^\beta)}{RT} \Rightarrow \mu_2(x_1^\alpha) = \mu_2(x_1^\beta) \quad (15)$$

According to Eqs. (15) solutions with mole fractions x_1^α and x_1^β are in *equilibrium* or, equivalently, the phases defined by the compositions x_1^α and x_1^β meet the *necessary phase equilibrium conditions*. Let us now consider a particular phase with a composition x_1^* located between x_1^α and x_1^β. As shown in Figure 6, for this phase the value of $\Delta\widetilde{G}/RT$ is negative, however, the same composition has a *lower value when located on the tangent line* (point B). The $\Delta\widetilde{G}/RT$ function represents the potential energy of thermodynamic systems and systems are globally stable when they have the lowest possible value of $\Delta\widetilde{G}/RT$ at a given composition. Point A represents the Gibbs energy of *a*

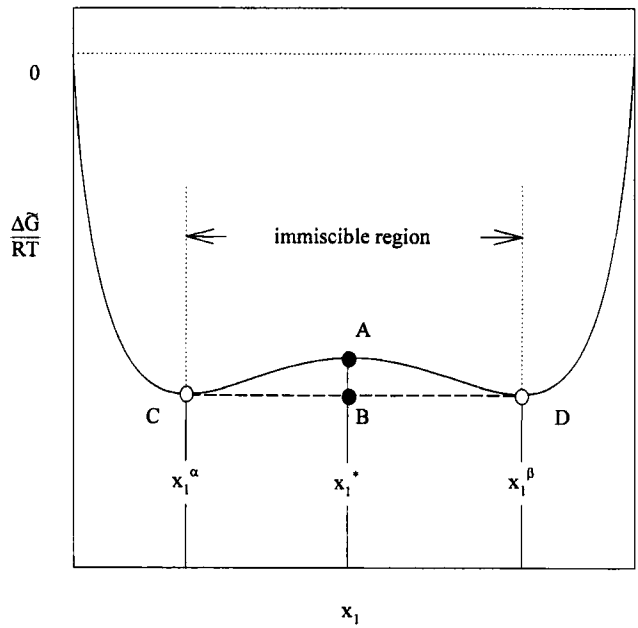

FIGURE 6 $\Delta\widetilde{G}/RT$ diagram characterizing the immiscibility ranges in Figure 5.

homogeneous phase for the mixture while point B represents the Gibbs energy of *two partially miscible phases* of composition x_1^α and x_1^β, respectively, with an overall composition x_1^*. From an energetic viewpoint, the composition x_1^* will favor the state with the lowest value of $\Delta\widetilde{G}/RT$ and it will be stable as a heterogeneous mixture of two immiscible phases of compositions x_1^α and x_1^β (point B), and not as a homogeneous phase (point A). In other words, a solution of composition x_1^* is unstable as a single phase, and represents a case of partial miscibility between two phases. The tangent line which joins x_1^α and x_1^β represents the *lever rule* and can be used to calculate the fraction of phases α and β (ψ_α and ψ_β):

$$\psi^\alpha = \frac{\overline{\mathrm{BD}}}{\overline{\overline{\mathrm{CD}}}} \quad \text{and} \quad \psi^\beta = \frac{\overline{\mathrm{CB}}}{\overline{\overline{\mathrm{CD}}}} \tag{16}$$

Equations (16) may be used for material balance purposes. Now, if a composition x_1^* is selected, subject to $x_1^* < x_1^\alpha$ or $x_1^* > x_1^\beta$, then Eqs. (16) will yield negative values for ψ^α and ψ^β, indicating that compositions in the range $x_1^* < x_1^\alpha$ or $x_1^* > x_1^\beta$ *cannot* represent a two-phase equilibrium state. Every composition x_1^* outside of the composition range CD corresponds to a homogeneous phase. A system that shows the behavior in Figure 6 is partially miscible, due to stability requirements. We have mentioned before that the curve in Figure 6 shows inflection points where the concavity of the $\Delta\widetilde{G}/RT$ curve changes sign from negative to positive. Hence, an additional miscibility test for a single-phase state in the *entire* composition range of a binary mixture can be obtained if the following condition is met, at constant temperature and pressure,

$$\left[\frac{\partial^2 \Delta\widetilde{G}/RT}{\partial x_1^2}\right]_{T,P} > 0 \tag{17}$$

for every possible composition. Equation (17) follows from the fact that a system will always present instability if $\Delta\widetilde{G}/RT$ inflects. In such a case it will always be possible to draw a common tangent joining immiscible compositions.

Next we will analyze the *hierarchy* of global and intrinsic stability. According to the latter, a system is stable if it yields a minimum of

Gibbs energy at constant temperature and pressure. Consider the state described by point A in Figure 7, which can be perturbed in many ways. One possibility is to unmix the original homogeneous mixture into two homogeneous mixtures of different compositions, such as B and C (a *small-scale perturbation*). According to the lever rule, the Gibbs energy of mixing of the unmixed system will be located in D resulting in a larger Gibbs energy. Hence, the result of the evolution of the system under such perturbation (B−C) will be to recover the original homogeneous composition given by point A. A larger perturbation is illustrated by unmixing the original solution A to the compositions given by points E and F (common tangent). In this case the Gibbs energy of mixing of the unmixed system will be located in H where it has a lower value. By being more stable than point A it will remain at this point. A solution of composition A is stable when it is subject to small perturbations and thermodynamics laws allows it. It will become unstable when the perturbations are large,

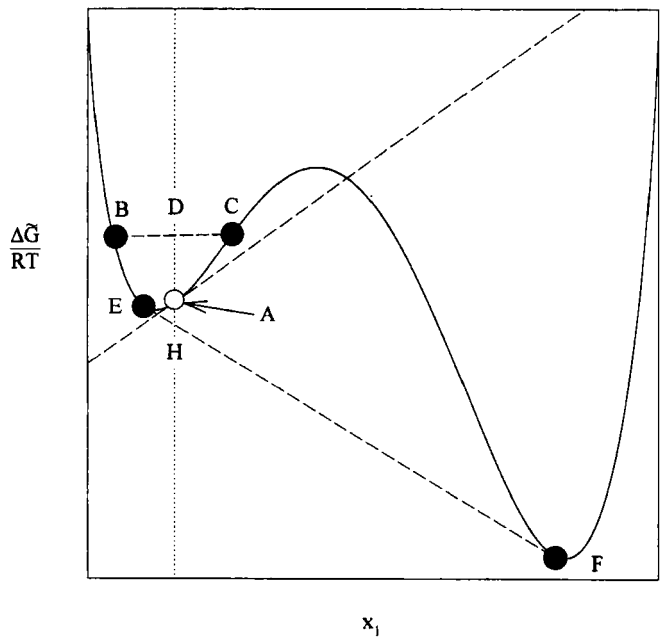

FIGURE 7 $\Delta\tilde{G}/RT$ diagram showing the ranges of metastability and global stability.

particularly since point H is the lowest Gibbs energy state among all the permissible mixing Gibbs energy states of the system that are given by the solid curve. Point A represents a case of metastability, *i.e.*, a miscible state which remains stable when subjected to small perturbations, but becomes unstable when subject to large perturbations. It is interesting to note that it is always possible to unmix a homogeneous state yielding larger mixing energies, as in case B–C, if the composition of the homogeneous mixture meets the condition given by Eq. (17). However, from a global stability viewpoint, the common tangent may include ranges of composition in the $\Delta\widetilde{G}/RT$ curve that will satisfy Eq. (17) but still yield lower values of the Gibbs function if the system becomes immiscible. A mixture having a composition that satisfies Eq. (17) is intrinsically stable as a homogeneous phase. If the composition of such a phase is *outside* the range of the common tangent no perturbation will be able to induce immiscibility and the homogeneous state will be globally stable. Considering again composition A, we can say that a homogeneous phase of such composition is intrinsically stable but not globally stable. A is inside the composition range of the common tangent and lower Gibbs energies can be achieved at point H. The important point to realize is that global stability always implies intrinsic stability, but intrinsic stability *does not* imply global stability.

Equation (17) may be also written as

$$\left[\frac{\partial^2 \widetilde{G}/RT}{\partial x_1^2}\right]_{T,P} > 0 \tag{18}$$

indicating that the Gibbs energy exhibits a positive concavity and thus, the stationary point of the Gibbs energy (required for an equilibrium state) is a minimum. But, as shown in the example given in Figure 7, Eq. (18) alone is unable to declare the *global stability* of the system with a given composition, when subject to large perturbations. The latter condition comes from the analysis of the tangent line to the Gibbs energy curve for the composition under study. As indicated before, composition A in Figure 7 exhibits intrinsic stability but not global stability. In addition, it is seen that the tangent at A exhibits composition ranges that are above the $\Delta\widetilde{G}/RT$ curve, so that some unmixing perturbations of the mixture with composition A are

possible, and for which the system could evolve to states with lower energies. Also, it can be seen that a tangent line at compositions outside the range E–F, where the mixture is a homogeneous phase, will always be *below* the $\Delta\widetilde{G}/RT$ curve. Hence, as established by the tangent line criterion [9], a mixture with a given composition is *globally stable* if the tangent line to the $\Delta\widetilde{G}/RT$ curve, in the pertinent composition, is *below* the $\Delta\widetilde{G}/RT$ curve in the full composition range.

Michelsen [10] has suggested that the tangent plane criterion be replaced by a *distance function* from the tangent line in a composition analysis to the $\Delta\widetilde{G}/RT$ curve. The tangent line at composition x_1^*, for a binary system, is given by:

$$C_{tg} = x_1 \frac{\Delta\overline{G}_1^*}{RT} + x_2 \frac{\Delta\overline{G}_2^*}{RT} \tag{19}$$

where $\Delta\overline{G}_i^*$ indicates the partial mixing Gibbs energy of the mixture at the given composition. In addition, for every composition the mixing Gibbs energy can be calculated from its partial properties according to

$$\frac{\Delta\widetilde{G}}{RT} = x_1 \frac{\Delta\overline{G}_1}{RT} + x_2 \frac{\Delta\overline{G}_2}{RT} \tag{20}$$

Thus the distance function for a stable mixture may be defined also as

$$\mathfrak{I} = \frac{\Delta\widetilde{G}}{RT} - C_{tg} = \sum_{i=1}^{2} x_i \left[\frac{\Delta\overline{G}_i}{RT} - \frac{\Delta\overline{G}_i^*}{RT} \right] \tag{21}$$

The global stability constraint establishes that the tangent should be below the $\Delta\widetilde{G}/RT$ curve hence, the global stability criterion may be also written

$$\mathfrak{I} = \sum_{i=1}^{2} x_i \left[\frac{\Delta\overline{G}_i}{RT} - \frac{\Delta\overline{G}_i^*}{RT} \right] \geq 0 \tag{22}$$

for every composition. Equations (17) and (22) show that the partial Gibbs energy function is a key property for stability analysis, and it can be calculated from thermodynamic models, as shown below. The partial Gibbs energy is defined in terms of fugacity as [15]

$$d\overline{G}_i = RTd\ln\hat{f}_i \tag{23}$$

Integrating Eq. (23) from the pure-component state to that of the mixture yields

$$\Delta\overline{G}_i = \overline{G}_i - \widetilde{G}_i = RT \ln \frac{\hat{f}_i}{f_i^0} \tag{24}$$

where f_i^0 is a pure-component fugacity reference for the i-th component. In stability analysis f_i^0 may be selected as hypothetical or real, according to convenience, for each component, but care must be taken that it be *the same fugacity reference* for every phase in which component i could exist. From Eqs. (20) and (24) we have

$$\frac{\Delta\widetilde{G}}{RT} = \sum_i x_i \frac{\Delta\overline{G}_i}{RT} = \sum_i x_i \ln \frac{\hat{f}_i}{f_i^0} \tag{25}$$

In the applications that follow the global stability analysis will be illustrated for various cases of heterogeneous phase equilibrium.

Stability and Liquid–Liquid Equilibrium in the $\gamma-\gamma$ Approach

In general, LLE is treated using activity coefficient models at low pressures. Using the Lewis and Randall reference state [15] the fugacity may be expressed as

$$\hat{f}_i = x_i \gamma_i f_i \tag{26}$$

where f_i is the pure component fugacity at the temperature and pressure of the mixture. As indicated before, a reference fugacity f_i^0 common to every phase is required in order to apply the global stability analysis. An appropriate selection is $f_i^0 = f_i$, for which substitution in Eq. (24) yields

$$\frac{\Delta\overline{G}_i}{RT} = \ln[\gamma_i x_i] \tag{27}$$

and the Gibbs energy of mixing is given by

$$\frac{\Delta\widetilde{G}}{RT} = \sum_i \frac{\Delta\overline{G}_i}{RT} = \sum_i x_i \ln[\gamma_i x_i] = \frac{\widetilde{G}^E}{RT} + \sum_i x_i \ln x_i \tag{28}$$

Equation (28) is the required relation for the stability analysis of a liquid mixture and yields a continuous and unique $\Delta\widetilde{G}/RT$ curve, due to the continuity of G^E models on composition.

Figure 8 shows an instructive construction of the LLE diagram using global stability concepts. Various isotherms of the $\Delta\widetilde{G}/RT$ curve have been plotted and for each isotherm the equilibrium tangent has been determined, together with the equilibrium compositions. This procedure allows to project equilibrium compositions in a $T-x$ LLE diagram. Although this procedure is not very accurate it allows an easy visualization of the equilibrium behavior and its relation with global stability. In addition, it may be used for initializing rigorous calculations that usually are nonlinear.

Stability analysis is *largely relevant* for the correlation of immiscibility data. Inspection of Figure 8 shows that the $\Delta\widetilde{G}/RT$ function inflects at two compositions inside the range of immiscibility, as required from stability conditions for immiscibility equilibrium, however, more than two inflections *are also possible*. Examples of the this situation have been given for the NRTL model [16] by Guffey and Wehe [17], Heidemann and Mandhane [18], Katayama *et al.* [19], and by Mattelin and Verhoye [20]. Wisniak and Segura [21] have illustrated a similar situation for the Gothard equation [22, 23]. It should be noted that NRTL is one of the models selected by the DECHEMA Chemistry Data Series [24] for correlating their experimental LLE database. In addition, Wisniak and Segura [21] have demonstrated the potential and flexibility of the Gothard equation for the treatment of common and extremely complex binary LLE data.

The existence of multiple inflections in the $\Delta\widetilde{G}/RT$ function may give place to potential pitfalls, as discussed below. Considering Eq. (26), the condition of equal chemical potentials may be expressed as

$$\mu_i^{\alpha} = \mu_i^{\beta} \Leftrightarrow x_i^{\alpha}\gamma_i^{\alpha} = x_i^{\beta}\gamma_i^{\beta} \tag{29}$$

For a binary system the compositions of immiscibility meet the following relation

$$\ln\frac{\gamma_1^{\alpha}}{\gamma_1^{\beta}} = \ln\frac{x_1^{\beta}}{x_1^{\alpha}}$$

$$\ln\frac{\gamma_2^{\alpha}}{\gamma_2^{\beta}} = \ln\frac{1-x_1^{\beta}}{1-x_1^{\alpha}} \tag{30}$$

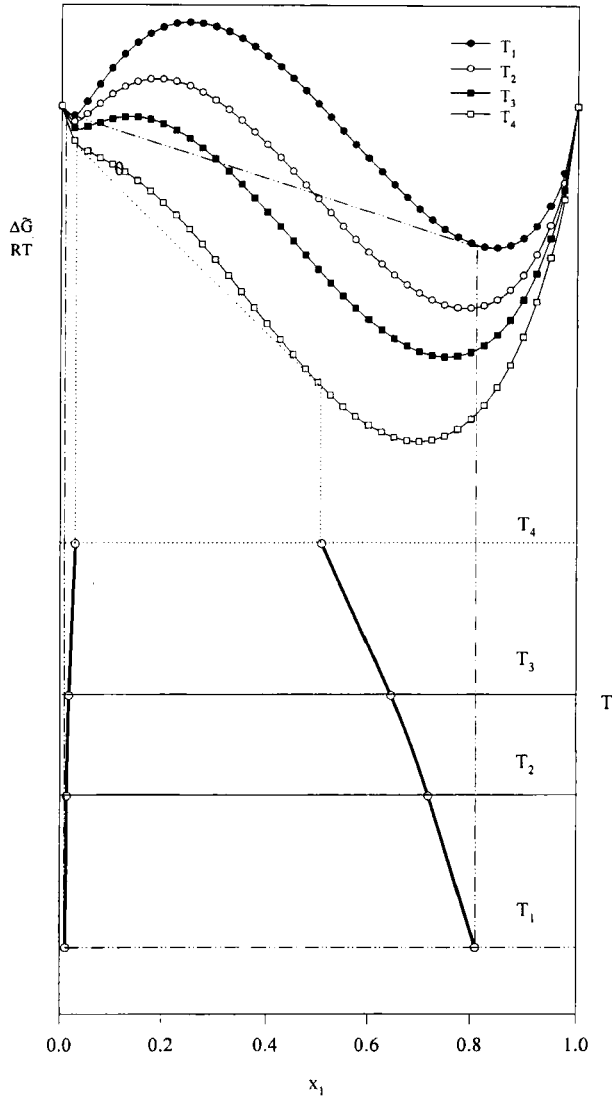

FIGURE 8 $\Delta\tilde{G}/RT$ diagram for a LLE in a $\gamma-\gamma$ approach showing the relation with the pertinent equilibrium diagram.

useful for correlating LLE. Equations (30) constitute a system of two equations, which may be solved in two unknowns parameters of a particular G^E model [21]. However, Eqs. (30) represent only *necessary* conditions for phase equilibrium, they do not consider either intrinsic

or global stability. Figure 9a presents a pathologic example of a $\Delta\tilde{G}/RT$ function with various inflections. The sign of the concavity requirement expressed in Eq. (18), indicates that compositions in the neighborhood of points B and D are intrinsically unstable; in addition, compositions in the neighborhood of points A, C and E are intrinsically stable but not globally stable. Figure 9a shows all the possible tangents that may be drawn; all of them satisfy Eqs. (29) and (30). Nevertheless, only those tangents that touch the curve at compositions that are intrinsically stable (like A, C, E), represent intrinsically stable equilibriums. Tangents that touch the $\Delta\tilde{G}/RT$ function in the neighborhood of point C are above the $\Delta\tilde{G}/RT$ curve in some composition ranges, as shown in Figure 9a, thus violating global stability. Therefore, Figure 9a represents a unique global stable equilibrium which

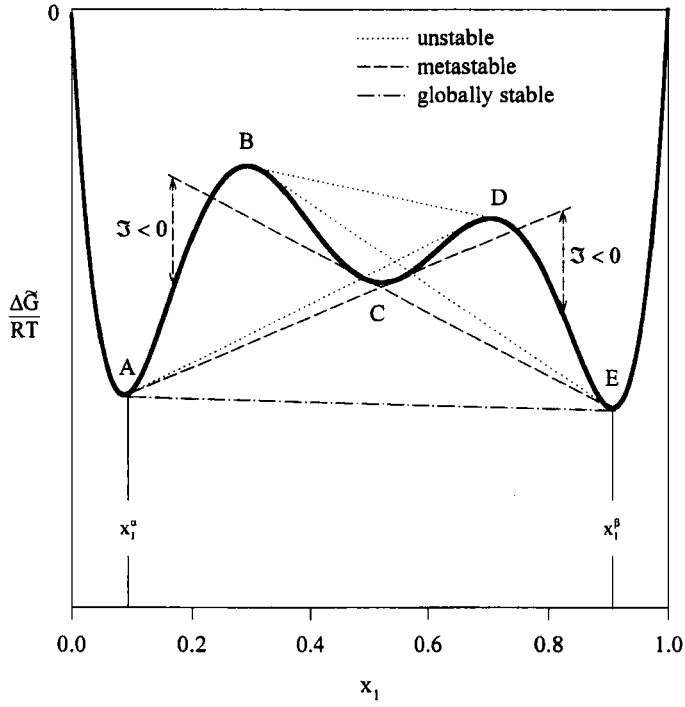

FIGURE 9a $\Delta\tilde{G}/RT$ diagram showing various inflections and possible tangents satisfying necessary phase equilibrium conditions.

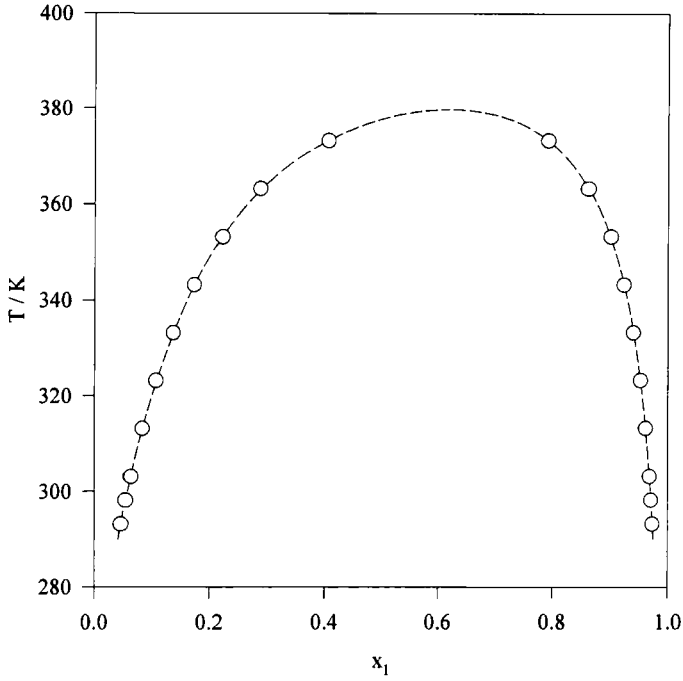

FIGURE 9b LLE diagram correlation for the system furfural (1) + 2,2,5-trimethylhexane (2) using the NRTL model. Experimental data taken from DECHEMA Chemistry Data Series [34] [o]. Model prediction *avoiding stability analysis* [—].

appears in the tangent that joins points A and E. Globally stable immiscibility will be observed *inside* the composition range AE.

The LLE data of the system furfural (1) + 2,2,5-trimethylpentane (2) [24] will be used to illustrate potential pitfalls which may be founded when fitting the data with the NRTL model, for example. For a binary system the NRTL model is

$$\frac{\tilde{G}^E}{RT} = x_1 x_2 \left[\frac{\tau_{21} G_{21}}{x_1 + x_2 G_{21}} + \frac{\tau_{12} G_{12}}{x_1 G_{12} + x_2} \right] \tag{31}$$

where

$$\begin{aligned} \tau_{ij} &= \frac{A_{ij}}{RT}; \quad A_{ij} = 0 \text{ if } i = j \\ G_{ij} &= \exp(-\alpha_{ij}\tau_{ij}); \quad \alpha_{ij} = \alpha_{ji} \end{aligned} \tag{32}$$

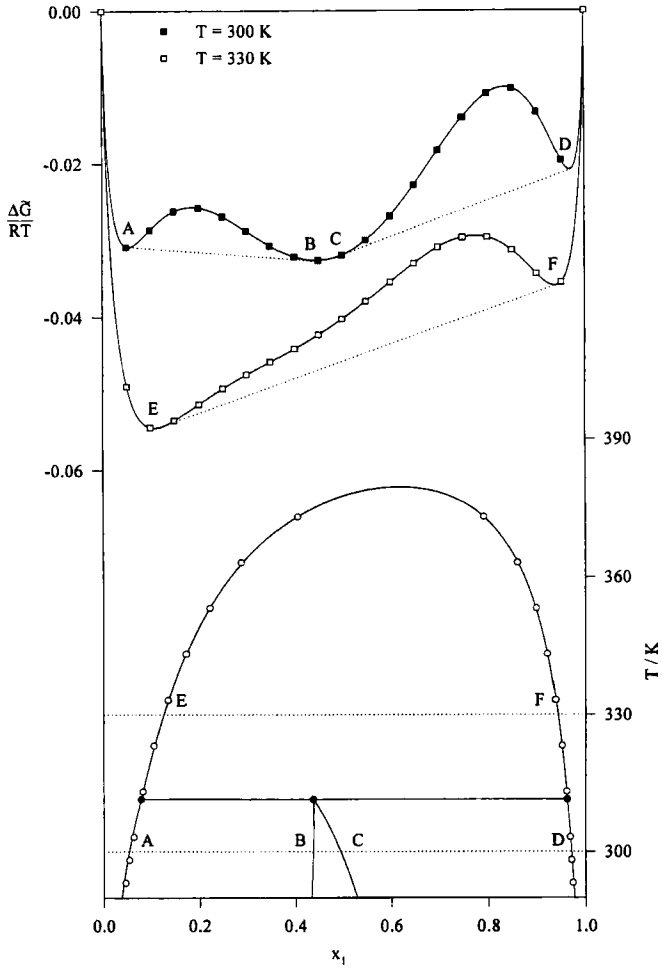

FIGURE 9c Stable LLE diagram prediction for the system furfural (1) + 2,2,5-trimethylhexane (2) using the NRTL model. Experimental data taken from Syrensen and Arlt [34] [o]. Model prediction *including stability analysis* [—].

The model parameters are A_{12}, A_{21}, and α_{12}. Eqs. (30) and the experimental immiscibility compositions may be used to solve Eqs. (31) and (32) for the two parameters A_{12} and A_{21}, if a constant value is assigned to α_{12}. Table I reports the values of these parameters for $\alpha_{12} = 0.42$. Figure 9b shows the ability of the NRTL model to predict the LLE of the system when only the necessary conditions of phase equilibrium

TABLE I Inappropriate NRTL fit parameters for the LLE of the system furfural (1) + 2,2,5-trimethylhexane (2)[a]

Coefficient	A_{12}/R	A_{21}/R
B_0	-1.7830×10^4	-2.2551×10^4
B_1	$+2.3438 \times 10^2$	$+3.3109 \times 10^2$
B_2	-1.0874	-1.7008
B_3	$+2.2463 \times 10^{-3}$	$+3.8156 \times 10^{-3}$
B_4	-1.7621×10^{-5}	-3.1877×10^{-5}

$$A_{ij}/R = B_0 + B_1 T + B_2 T^2 + B_3 T^3 + B_4 T^4$$

[a] data taken from *DECHEMA Data Series* [24].

are satisfied, and Figure 9c shows the prediction when stability analysis is taken into consideration. The obvious conclusion is that the model and the fitted parameters predict a behavior that is *not observed* in the experimental data at low temperatures. Figure 9c shows that the $\Delta\widetilde{G}/RT$ function presents multiple inflections, so that the equilibrium diagram shown in Figure 9b, although depicting an excellent correlation of the data, is not globally stable in the low temperature range.

Stability and Vapor–Liquid Equilibrium in the $\gamma - \phi$ Approach

According to the $\gamma - \phi$ approach, VLE equilibrium compositions satisfy the relation

$$x_i \gamma_i f_i = y_i \hat{\phi}_i P \tag{33}$$

where f_i is the pure liquid fugacity given by

$$f_i = P_i^{\text{sat}} \phi_i^{\text{sat}} \upsilon_i \tag{34}$$

In Eq. (34) P_i^{sat} is the vapor pressure, ϕ_i^{sat} the pure component fugacity coefficient at saturation conditions and υ_i is the Poynting factor defined as

$$\upsilon_i = \exp\left[\frac{\tilde{v}_i^L}{RT}(P - P_i^{\text{sat}})\right] \tag{35}$$

In the $\gamma - \phi$ approach the fugacities of the vapor and liquid phases are independently modeled using virial EOS and G^E models, according

to the following relations

$$\hat{f}_i^V = y_i \hat{\phi}_i P$$
$$\hat{f}_i^L = x_i \gamma_i f_i^0 \tag{36}$$

Therefore, selecting $f_i^0 = f_i$ as the reference fugacity, we obtain from Eq. (24)

$$\Delta \overline{G}_i^V = RT \ln \frac{\hat{f}_i^V}{f_i} = RT \ln \frac{y_i \hat{\phi}_i P}{f_i} \tag{37a}$$

$$\Delta \overline{G}_i^L = RT \ln \frac{\hat{f}_i^L}{f_i^0} = RT \ln \frac{x_i \gamma_i f_i}{f_i} \tag{37b}$$

The pertinent $\Delta \widetilde{G}/RT$ curves for each phase, written as functions of the composition x_i, are

$$\frac{\Delta \widetilde{G}_i^V}{RT} = \sum_i x_i \frac{\Delta \overline{G}_i^V}{RT} = \sum_i x_i \ln \frac{x_i \hat{\phi}_i P}{f_i^0} \tag{38a}$$

$$\frac{\Delta \widetilde{G}_i^L}{RT} = \sum_i x_i \frac{\Delta \overline{G}_i^L}{RT} = \frac{\widetilde{G}^E}{RT} + \sum_i x_i \ln x_i \tag{38b}$$

It should be clear that Eqs. (38a) and (38b) are *not* equivalent functions of the composition; their evaluation at constant T and P will give a different $\Delta \widetilde{G}/RT$ curve for each phase. In addition, it should be noted that when the pressure increases, $\Delta \widetilde{G}^V/RT$ also increases (considering moderate pressures and conditions far from the critical range), indicating that at higher pressures the vapor phase becomes less stable, an observation consistent with the isothermal condensation of a vapor at the dew-point pressure.

Figure 10 shows the values of $\Delta \widetilde{G}/RT$ and the equilibrium diagram for a VLE situation at a constant temperature T and pressure P^*. The $\Delta \widetilde{G}/RT$ curves for the liquid and vapor phases appear in the upper region of the figure where it can be seen that each phase is represented by its own $\Delta \widetilde{G}/RT$ curve, as required by Eqs. (38a) and (38b). For every composition in the range A–E the curve $\Delta \widetilde{G}^L/RT$ is below

$\Delta\tilde{G}^V/RT$, indicating that in this range the liquid phase is more stable. The vapor phase becomes more stable for compositions in the range E–D. In addition, every tangent line drawn to the lower $\Delta\tilde{G}/RT$ curve for compositions located in the range B–C, intersects the more stable $\Delta\tilde{G}/RT$ curve at some composition (as shown by the tangent line F–G). From this we infer that the composition range B–C is not *globally* stable for a homogeneous phase. The liquid and vapor phase $\Delta\tilde{G}/RT$ curves meet the common tangent line at compositions B and C; thus phases of such compositions are in equilibrium, as discussed for Figure 4. Consequently, the composition range A–B represents homogeneous liquid mixtures, the range B–C is a range of *global instability for homogeneous phases* where VLE is present, and the range C–D represents homogeneous vapor mixtures. Furthermore, and as expected, the results of the stability analysis match exactly the conditions observed in the P^* isobar in the VLE diagram projected in the lower region of Figure 10.

As shown by the example in Figure 10, VLE introduces new featuresin the stability analysis, particularly the fact that phases of substantially different densities (in this case, liquid and vapor) are represented *by different* $\Delta\tilde{G}/RT$ *curves*. In addition, although global stability criteria apply straightforward, the case warrants further inspection. For example, it is clear from Figure 10 that the $\Delta\tilde{G}/RT$ curves of both liquid and vapors phases meet the intrinsic stability criterion expressed by Eq. (18). In principle, *homogeneous vapor and liquid phases could exist in the whole composition range*, although being metastable for some compositions. In the example under consideration the homogeneous liquid phase is metastable in the composition range B–D and the homogeneous vapor phase is metastable in the range A–C. Furthermore, as compared with typical LLE cases, in VLE it is *not necessary for the concavity of* $\Delta\tilde{G}/RT$ *to change sign* to induce a phase equilibrium state.

Of particular interest in VLE stability analysis is the case of heteroazetropy where liquid–liquid immiscibility appears in addition to a vapor phase in equilibrium with both liquid phases. The typical case of heteroazetropy is shown in Figure 11 where two isobars ($P_1 > P_2$) of the $\Delta\tilde{G}^V/RT$ curve have been plotted to show how the heteroazetropic diagram may be deduced from global stability arguments. The upper region of the Figure shows the $\Delta\tilde{G}/RT$ plot and the

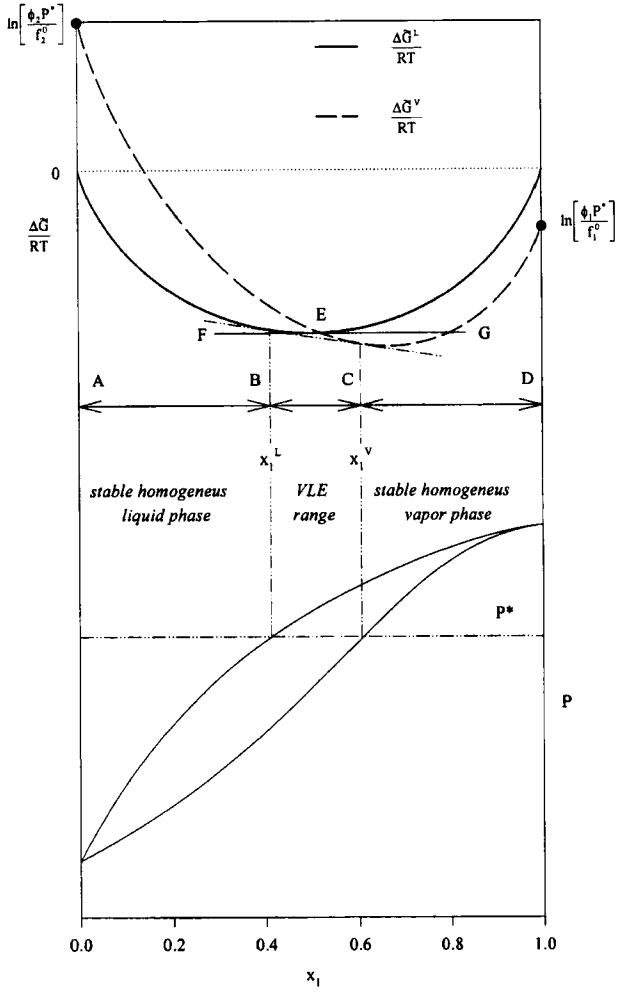

FIGURE 10 $\Delta\tilde{G}/RT$ diagram for a VLE in a $\gamma-\phi$ approach showing the relation with the pertinent equilibrium diagram.

lower region depicts the projected equilibrium diagram. Equations (38) indicate that only $\Delta\tilde{G}^V/RT$ depends on pressure. $\Delta\tilde{G}^L/RT$ may depend on pressure if G^E considers functionality explicit in excess volumes, but usually this is not the case because at low pressures G^E models depend only on temperature and composition. At the heteroazeotropic pressure P_1 two liquid-phase compositions and one

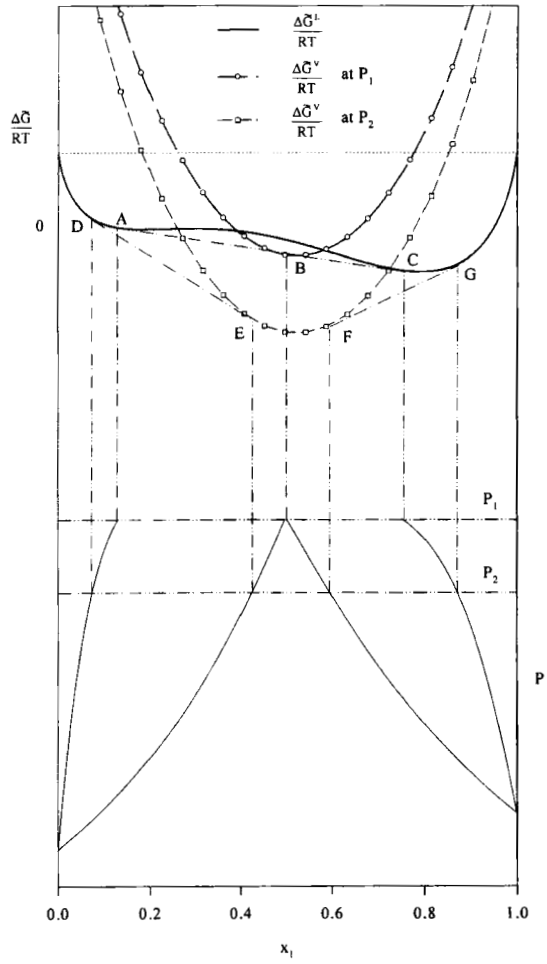

FIGURE 11 $\Delta\tilde{G}/RT$ diagram for a VLE in a $\gamma-\phi$ approach showing a case of hetero-azeotropy.

vapor-phase composition meet the common tangent line ABC, indicating that these compositions are in phase-equilibrium conditions. When the pressure is reduced to P_2 it is possible to find two composition ranges, D–E and F–G, inside of which global instability is observed. The pertinent tangents give place to VLE in the two composition ranges D–E and F–G.

Liquid phase immiscibility at heteroazeotropic (and higher) pressures is a consequence of the inflection of $\Delta\widetilde{G}^L/RT$. False and narrow immiscibility gaps may predicted by models when analyzing binary VLE data that exhibit large positive deviations from ideal behavior [25], affecting consistency analysis [2], data reduction, and multicomponent VLE predictions. Stability analysis should be used for testing the capabilities of particular models, in order to correlate adequately a particular set of data. An appropriate methodology may be to analyze the concavity of $\Delta\widetilde{G}^L/RT$ for the G^E model fitted to the data. Changes in the sign of the $\Delta\widetilde{G}^L/RT$ curve concavity are indicative of immiscibility gaps and, if heteroazeotropy is not present in the experimental data, a model that shows inflections should be judged as *inappropriate for correlation purposes.*

Stability and Phase Equilibrium in the $\phi-\phi$ Approach

The $\phi-\phi$ approach to phase equilibrium is related to an EOS being able or representing simultaneously vapor and liquid phases, the most common case being a cubic EOS of the van der Waals type. Such an approach may be used for representing every case of phase equilibrium between fluid phases, including critical transitions. Accuracy of the representation will depend mainly on the EOS selected and it's mixing rules. In the $\phi-\phi$ approach, the necessary condition of phase equilibrium may be expressed as

$$x_i^\alpha \hat{\phi}_i^\alpha = x_i^\beta \hat{\phi}_i^\beta = \cdots\cdots \tag{39}$$

where $\hat{\phi}_i$ is the fugacity coefficient of a component in a mixture. The fugacity coefficient may be calculated from residual properties, defined as

$$\widetilde{M}^R = \widetilde{M}(T,P) - \widetilde{M}^{ig}(T,P) \tag{40}$$

$\ln\hat{\phi}_i$ is related to the partial residual Gibbs energy and may be calculated from volumetric data as follows [15]

$$\ln\hat{\phi}_i = \frac{\overline{G}_i^R}{RT} = \int_0^P \left(\frac{\overline{Z}_i - 1}{P}\right) dP = \left(\frac{\partial n\widetilde{A}^R/RT}{\partial n_i}\right)_{T,n\bar{v},n_j} - \ln Z \tag{41}$$

In Eq. (41) Z is the compressibility factor and $\tilde{A}^R$ is the residual Helmholtz energy which may be calculated from the relation [15]

$$\frac{\tilde{A}^R}{RT} = \int_{\tilde{v}}^{\infty} \left[\frac{P}{RT} - \frac{1}{\tilde{v}} \right] d\tilde{v} \tag{42}$$

Equation (42) is particularly useful for an EOS of the form $P = P(T, V, n)$. Solutions of Eqs. (41) and (42) that can be applied to common EOS and mixing rules for pure compounds, mixtures and for each of their components, appear in Appendix I.

There are additional complications when an EOS is used to calculate fugacity coefficients. At a given T, P and composition, an EOS may give one or three real volumetric roots larger than the minimum packing volume or covolume. This root multiplicity is a consequence of the van der Waals loop and appears in every EOS derived from perturbation theories [14]. When an EOS gives three real roots larger than the covolume, the smallest represents a liquid-type root, the largest a gas-type root, and the central has no physical meaning because it violates the mechanical stability criteria:

$$\left(\frac{\partial P}{\partial V} \right)_T < 0 \tag{43}$$

Equation (43) establishes a well-known compressibility property of a real fluid. Consequently, an EOS applied to pure components may give a multiplicity of fugacity coefficients, each one related to a particular volume. Considering Eq. (41) and the definition of residual property given by Eq. (40), the pure component fugacity coefficient is

$$\frac{\tilde{G}_i^R}{RT} = \frac{\tilde{G}_i}{RT} - \frac{\tilde{G}_i^{ig}}{RT} = \ln \phi_i \tag{44}$$

Selecting the fugacity having the *minimal* value assures the lowest Gibbs energy and, as follows from stability considerations, such minimal fugacity coefficient may be associated to a stable phase (as predicted by the EOS). Therefore, an appropriate selection for the pure component fugacity reference is:

$$\ln \phi_i^0 = \min[\ln \phi_i]_{T,P} \tag{45}$$

where $[\ln \phi_i]$ represents the set of pure component fugacity coefficients obtained at a given temperature and pressure.

In the $\phi-\phi$ approach, the fugacity of a component in a mixture is given by

$$\hat{f}_i^{\pi} = x_i^{\pi} \hat{\phi}_i^{\pi} P \tag{46}$$

for every phase ($\pi = L, V$). Application of Eq. (46) to a pure component yields the pure component fugacity

$$f_i^{\pi} = \phi_i^{\pi} P \tag{47}$$

which may be selected as the reference fugacity ($f_i^0 = f_{i\pi}$). Therefore, considering Eqs. (47) and (46), Eq. (25) may be written as

$$\frac{\Delta \widetilde{G}}{RT} = \sum_i x_i \ln\left(\frac{x_i \hat{\phi}_i P}{f_i^0}\right) = \ln \phi_m - \sum_i x_i \ln \phi_i^0 + \sum_i x_i \ln x_i \tag{48}$$

where

$$\ln \phi_m = \sum_i x_i \ln \hat{\phi}_i \tag{49}$$

for each phase, and ϕ_i^0 is a pure component fugacity coefficient reference, all of them evaluated at same temperature and pressure. Equation (48) allows writing the Gibbs energy of mixing in terms of fugacity coefficients for each phase and, in addition, constitutes a criterion by which stability can be examined. An equivalent criterion is obtained from the distance of the tangent line to the $\Delta \widetilde{G}/RT$ curve, as discussed in Eq. (22). Replacing Eq. (48) in Eq. (22) yields the stability criteria, in terms of fugacity coefficients

$$\Im = \sum_i x_i(\ln[\hat{\phi}_i x_i] - \ln[\hat{\phi}_i^* x_i^*]) = \ln \phi_m - \sum_i x_i \ln \frac{\hat{\phi}_i^* x_i^*}{x_i} \geq 0 \tag{50a}$$

Equation (50a) represents a previous observation about Figure 7, the fact that a stable phase has a tangent that is always *below* the $\Delta \widetilde{G}/RT$ curve. Hence, the stability criterion for the tested point with concentration x_i^* has to be applied for all *auxiliary* concentrations x_i^A

in the range $0 < x_i^A < 1$, separately for each phase, at the same temperature and pressure. Thus the difference between the $\Delta\tilde{G}/RT$ curve and the tangent line for every composition point must be positive or zero, if the test phase of composition x_i^* is stable, as indicated by writing the second equality in Eq. (50a), as follows

$$\mathfrak{J} = \ln \phi_m^A - \sum_i x_i^A \ln \frac{\hat{\phi}_i^* x_i^*}{x_i^A} \geq 0 \tag{50b}$$

Equation (50b) may be used now to test the stability of a particular phase for *binary* and *multicomponent* mixtures [10].

The Soave modification of the van der Waals EOS [26] with classical mixing rules, will now be used to illustrate some important facts regarding the test of global stability using EOS (results are conceptually similar for other EOS and/or mixing rules). We will consider a solution of ethanol (1) + water (2) at 373.15 K, using the critical constants and acentric factors given in Table II. In addition, a zero interaction parameter (k_{ij}) will be used in the mixing rule. It should be pointed out that *this is not a good approximation for the system*, whose experimental data is not represented by the EOS under consideration with zero interaction parameter (in general this mixture cannot be well represented by standard cubic EOS with classical mixing rules, even when using non-zero interaction parameter. Advanced mixing rules are required for quantitative purposes). The phase equilibrium diagram predicted by the model is shown in Figure 12, where four isobars (P_A = 50 kPa, P_B = 150 kPa, P_C = 240 kPa and P_D = 300 kPa) have been selected to illustrate how the phases appear in a $\Delta\tilde{G}/RT$ diagram. Figure 13a shows the $\Delta\tilde{G}/RT$ diagram for P_A. ϕ_i^0 has been selected with Eq. (45) and three volumetric roots are obtained for the mixture in the full composition range, each one generating a $\Delta\tilde{G}/RT$ curve (some values of the volumetric roots are given in Tab. III). As

TABLE II Pure component properties for the mixture ethanol (1) + water (2)[a]

Component	T_c/K	P_c/kPa	ω
1	516.20	63.83	0.6350
2	647.30	220.48	0.3440

[a] Data taken from Reid *et al.* [30].

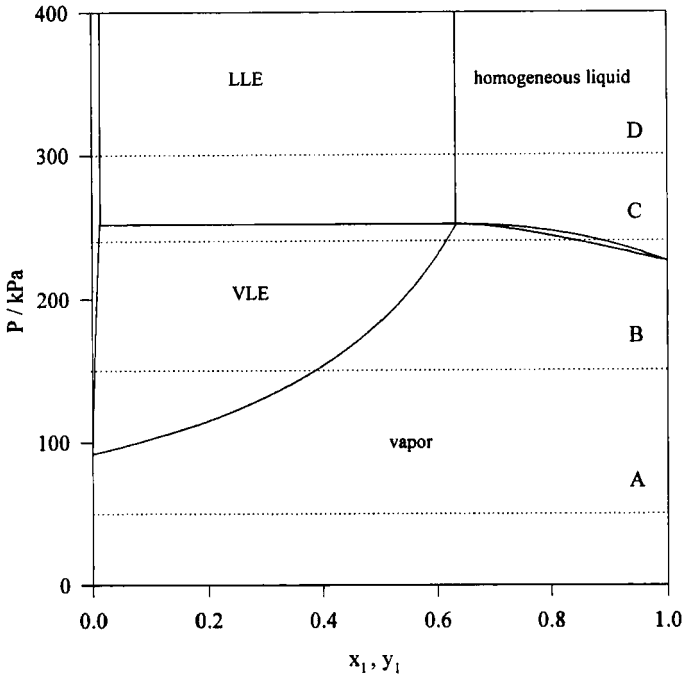

FIGURE 12 Prediction of vdW-S EOS for the system ethanol (1) + water (2) at 373.15 K ($k_{ij} = 0$).

shown by Figure 13a, for *every composition* $\Delta\tilde{G}^V/RT$ yields the lowest values and we conclude that only the vapor phase is globally stable at 373.15 K and P_A, as confirmed by the phase equilibrium diagram given in Figure 12. Note that the central root yields always the largest values of $\Delta\tilde{G}/RT$, due to the instability condition expressed by Eq. (43). Figure 13b shows the isobar P_B indicated in Figure 12. In this case we can plot the $\Delta\tilde{G}^L/RT$ and $\Delta\tilde{G}^V/RT$ curves, as well as a tangent, the latter touching $\Delta\tilde{G}^L/RT$ and $\Delta\tilde{G}^V/RT$ curves at the pertinent equilibrium compositions. This tangent corresponds to the VLE range shown in Figure 12 at P_B, inside this range a single phase qualifies as globally unstable. The figure shows also the $\Delta\tilde{G}/RT$ curve corresponding to the central volumetric root; this curve again yields the largest $\Delta\tilde{G}/RT$ values in the whole composition range and will be ignored in further analysis. Figure 13c shows the isobar P_C indicated in Figure 12. In this case the curves $\Delta\tilde{G}^L/RT$ and $\Delta\tilde{G}^V/RT$ intersect at two

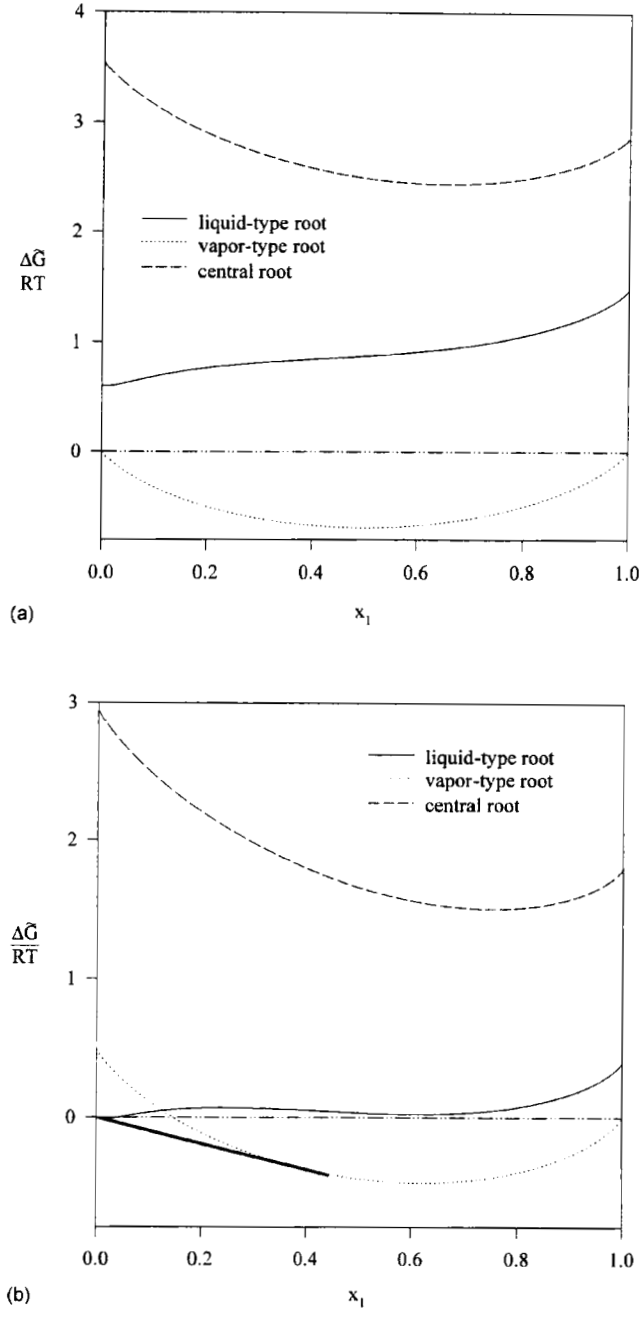

FIGURE 13 $\Delta\tilde{G}/RT$ plots for the various pressure levels shown in Figure 12. (a) P_A; (b) P_B; (c) P_C; (d) P_D.

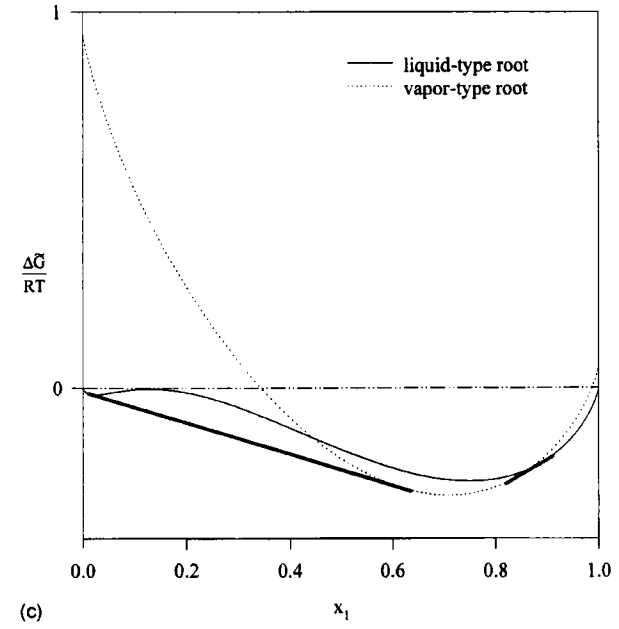

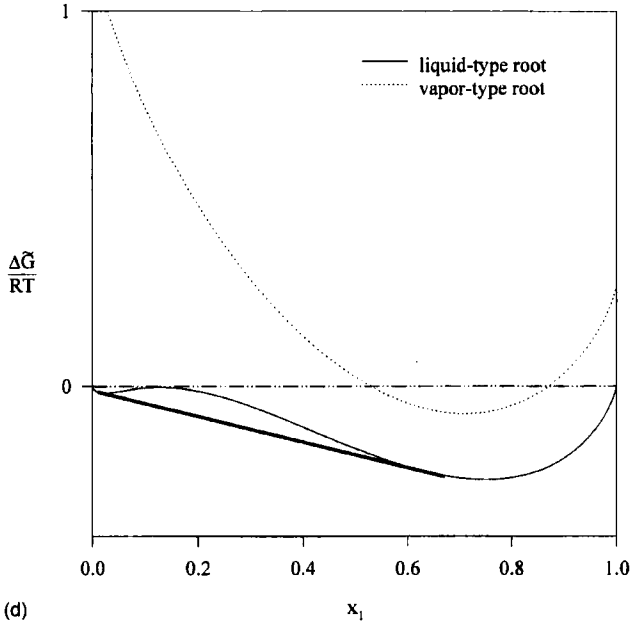

FIGURE 13 (Continued).

TABLE III Compressibility factor roots for Figure 13a

x_1	Z		
	Liquid	*Central*	*Vapor*
0.0	0.0006	0.0039	0.9960
0.1	0.0007	0.0042	0.9957
0.2	0.0008	0.0046	0.9953
0.3	0.0009	0.0049	0.9950
0.4	0.0010	0.0052	0.9946
0.5	0.0011	0.0056	0.9942
0.6	0.0012	0.0060	0.9938
0.7	0.0013	0.0064	0.9934
0.8	0.0014	0.0068	0.9929
0.9	0.0015	0.0073	0.9924
1.0	0.0016	0.0078	0.9920

different compositions and two equilibrium tangents can be plotted. According to Figure 12, there are two ranges of VLE and, again, every composition between the equilibrium compositions corresponds to a globally unstable single phase. In addition, although $\Delta\tilde{G}^L/RT$ inflects (*suggesting a clear case of immiscibility*), the LLE is not globally stable at P_C because the corresponding tangent is *above* the VLE tangent, resulting in higher values of the mixing Gibbs energy. Finally, Figure 13d shows the isobar P_D indicated in Figure 12, where only LLE is observed. This time the $\Delta\tilde{G}^V/RT$ curve appears above that of the liquid phase and thus the vapor phase is unstable. This result is obvious when the pressure is increased (below the critical range) because the vapor phase becomes unstable and eventually condenses. It should be noted that in going from Figure 13a to d the pressure increases, and that the vapor phase has higher $\Delta\tilde{G}/RT$ values, indicating that increasing pressures produce unstable vapors, as mentioned before.

Considering Figure 13a again, it is seen that the $\Delta\tilde{G}^L/RT$ curve inflects so that, in general, we can expect liquid immiscibility to be present. However, the vapor phase presents lower $\Delta\tilde{G}/RT$ values corresponding to a globally stable phase. Independently of previous considerations, it is possible to obtain a false (or metastable) LLE when solving only the necessary equilibrium condition given by Eq. (39) and ignoring the stability test. Results of such a calculation appear in Table IV.

Let us now to analyze how the criteria shown in Eq. (50b) can be applied avoid these false immiscible phases. At the composition of the

test phase is $x^* = x^\alpha$ and $\Im$ may be evaluated for all *possible compositions and compressibility roots* and the pertinent results are presented in Figure 14. It is seen that the test composition yields positive values for $\Im$ when considering the "phase" represented by the central root, the same fact is observed when the liquid phase is analyzed. However, in the case of the vapor phase it is clear that the test composition is not stable. *A test phase or composition is globally stable if, and only if, all the possible values that* $\Im$ *can yield for all the composi-*

TABLE IV LLE calculation at 373.15 K and $P = 50$ kPa (P_A in Fig. 10)

Component	x^α	x^β
	(*liquid* α *phase*)	(*liquid* β *phase*)
Ethanol (1)	0.0138	0.6356
Water (2)	0.9862	0.3644

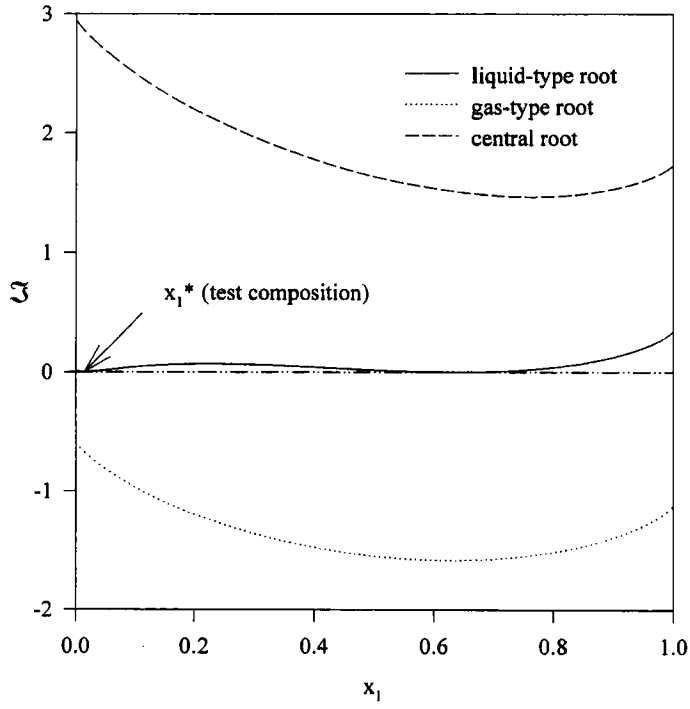

FIGURE 14 Application of the global stability criteria according to Eq. (50b).

tions and phases are positive. This is not the case in Figure 14; hence the test composition is not globally stable. The stability assessment is directly confirmed by the phase diagram given in Figure 12 because at $P_A = 50\,\text{kPa}$ no liquid phase exist. The LLE shown in Table IV is a *metastable equilibrium state predicted* by the model.

According to Figure 12, when the pressure increases to P_D, LL immiscibility is obtained (the pertiment calculation in shown in Tab. V). One of the immiscibility compositions, x_1^β, is tested now and the corresponding stability analysis is shown in Figure 15. It is seen that $\Im$ is always positive so the LLE can be declared *globally* stable. But if the same equilibrium composition is tested at $3 \times 10^5\,\text{kPa}$ and 373.15 K, it becomes unstable (see Fig. 16), indicating that LL immiscibility increases with pressure. Furthermore, as shown in Figure 16, the EOS predicts only liquid-type roots. Figures 13 to 16 include the main features that can be observed in the stability analysis with an EOS, results that in the subcritical range are not substantially different from those observed in the $\gamma-\phi$ approach. The only exceptions to the above rules are the way in which the reference value for the fugacity is selected. This example illustrates also some of the potential pitfalls which can be found when fitting interaction parameters to experimental data. For example, it is possible to obtain globally unstable LLE (as the case analyzed with P_A) by means of $\phi-\phi$ calculations and although the model can smooth the LLE data in this range, such parameter fit is not correct because the EOS qualifies a homogeneous vapor phase as globally stable.

The calculation of critical lines has acquired increasing interest after the basic work of Van Konyenburg and Scott [4] because it allows assessment of the predictive capabilities of an EOS in the critical range and an excellent approach to the topology of phase equilibrium diagrams in the whole PVT range. Critical calculations are directly related to conditions of intrinsic stability, as follows from the classical

TABLE V LLE calculation at 373.15 K and $P = 3\,\text{bar}$ (P_D in Fig. 10)

Component	x^α	x^β
	(*liquid α phase*)	(*liquid β phase*)
Ethanol (1)	0.0138	0.6356
Water (2)	0.9862	0.3644

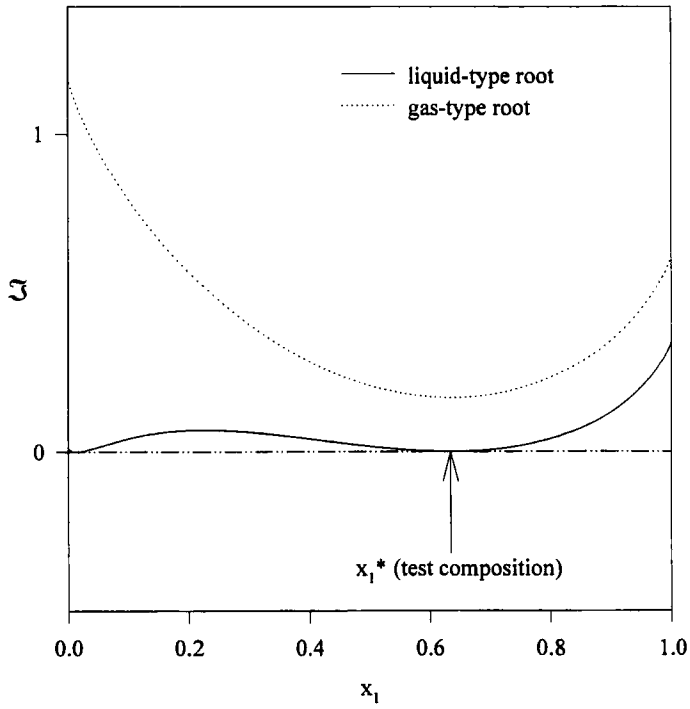

FIGURE 15 Stability test for a LLE of composition x_1^{β} at 300 kPa.

conditions of the critical point of mixtures. For a binary systems we have [27]

$$\left(\frac{\partial^2 \tilde{G}}{\partial x_1^2}\right)_{T,P} = 0; \quad \left(\frac{\partial^3 \tilde{G}}{\partial x_1^3}\right)_{T,P} = 0; \quad \left(\frac{\partial^4 \tilde{G}}{\partial x_1^4}\right)_{T,P} > 0 \qquad (51)$$

The composition derivatives of the Gibbs energy given by Eqs. (47) can be related to Helmholtz energy derivatives using a Legendre transformation [6], yielding an equivalent set of non-linear equations which can be directly applied to an EOS of the form $P = P(T, V, n)$. However, Eq. (51) do not take into account global stability and constitute only *necessary* conditions. Complete critical calculations must be complemented with global stability analysis along critical

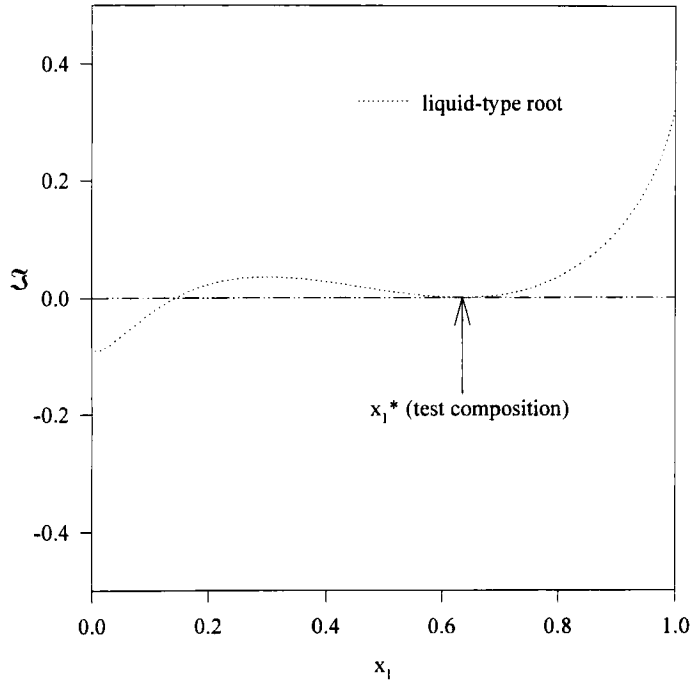

FIGURE 16 Stability test for a LLE of composition x_1^{β} (immiscibility composition at 300 kPa) at 3×10^5 kPa.

lines. In order to illustrate this important point, we have calculated the critical lines of the system ethanol (1) + water (2) using the vdW-S EOS, with zero interaction parameter. The pertinent results appear in Figure 17. As mentioned before the model is *not adequate* for this system and will be used only for illustration purposes. According to Figure 17 the system is predicted as Type II in the classification of Van Konynenburg and Scott [4], showing a sharp range of immiscibility below the critical temperatures of both components. In contrast, experimental results indicate that the system ethanol (1) + water (2) is Type I, completely miscible and with a positive azeotrope ending in the critical range. Anyhow, it is of interest to study the global stability of the prediction. Critical line calculations using Eq. (51) yield two critical lines, a gas–liquid critical line that joins continually the critical points of the pure components, and a liquid–liquid critical line that represents the upper consulate temperature of the immisci-

bility shown in Figure 12, extending from zero to infinite pressure. Both critical lines satisfy the limit of intrinsic stability because they satisfy Eq. (51) but, obviously, liquid states become globally unstable as pressure decreases. Therefore, it is reasonable to assume that the LLE critical line cannot start from zero pressure. Table VI includes the coordinates of the critical immiscibility of points A, UCEP, (upper critical end point), and B whose stability analysis is shown in Figure 18. As follows from Figure 18, the minimum pressure, which stabilizes

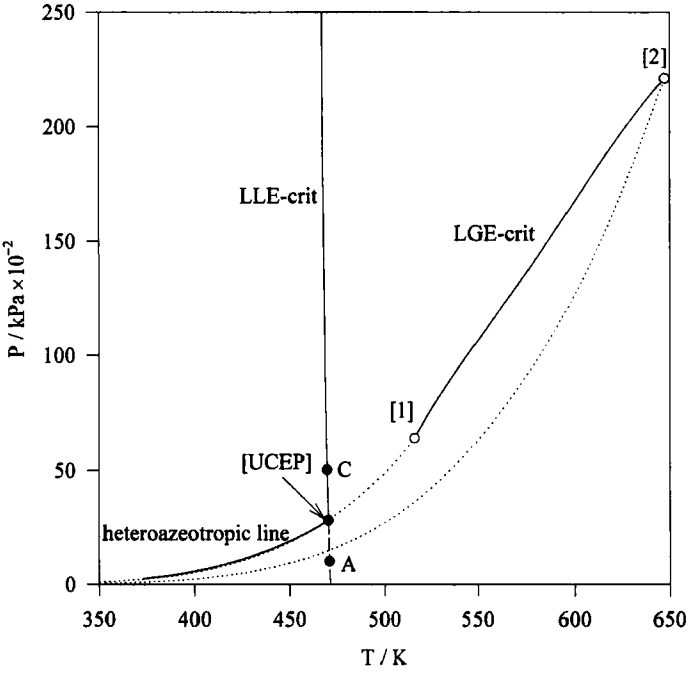

FIGURE 17 Critical $P-T$ projection predicted by the vdW-S EOS for the system ethanol (1) + water (2) [$k_{ij} = 0$].

TABLE VI Critical compositions of immiscibility along the LLE critical line in Figure 15

Point	T_c/K	P_c/bar	x_1^c
A	470.91	10.02	0.1675
UCEP	470.31	27.99	0.1673
C	469.68	50.18	0.1671

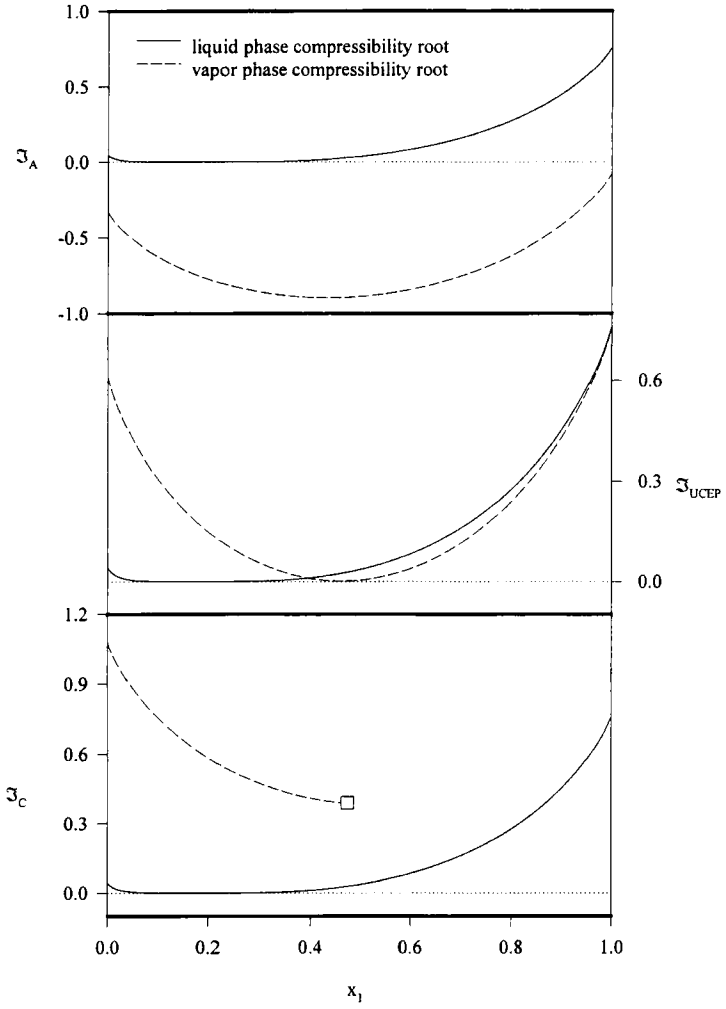

FIGURE 18 Stability analysis along the LLE critical projection shown in Figure 17.

a critical LLE, is the UCEP pressure, and the pressure range A-UCEP is metastable.

Stability Analysis in Solid–Fluid Equilibrium

Solid–fluid equilibrium is related with separation technologies where SFE becomes a potentially attractive purification alternative. This ap-

proach to separation problems is adequate with biological products, or with chemical species of large molecular weights that exhibit high boiling points, and usually decompose in normal distillation. Solutes of low volatility may be exposed to supercritical solvents, as carbon dioxide, at room temperature, avoiding thus thermal degradation.

The equilibrium condition for the low volatile solid solute (identified as component 2) is written in terms of fugacity as

$$\hat{f}_2^S = \hat{f}_2^{fp} \tag{52}$$

where S, and fp denote the solid and fluid phases, respectively. The fugacity of the solid phase is given approximately by the fugacity of pure solid [28] where the miscibility of the solvent is negligible

$$f_2^S = P_2^{VS}\phi_2^{\text{sat}} \exp\left[\frac{\tilde{v}^S}{RT}\left(P - P_2^{VS}\right)\right] \tag{53}$$

In Eq. (53) P_2^{VS} is the sublimation pressure and ϕ_2^{sat} and $\tilde{v}^S$ are the fugacity coefficient and the molar volume of the pure solid at sublimation conditions. The exponential term in the right-hand side of the equation represents the Poynting factor when the compressibility of the solid phase is neglected. A more rigorous approach can be obtained if the compressibility of the solid is known, but this kind of data is usually not available in the literature. The fugacity of each component in the fluid phase may be written

$$\hat{f}_i^{fp} = y_i\hat{\phi}_i P \tag{54}$$

where y_2 is the solubility and $\hat{\phi}_i$ is the gas phase fugacity coefficient which can be estimated from an EOS. The practical pressure ranges observed in supercritical extraction suggest the use of an EOS based on perturbation theories (*such as a cubic* EOS), instead of a virial EOS, for estimating gas phase fugacity coefficients. Combining Eqs. (53) and (54) and solving for the solubility yields

$$y_2 = \frac{P_2^{VS}\phi_2^{\text{sat}}}{P\hat{\phi}_2} \exp\left[\frac{\tilde{v}^S}{RT}\left(P - P_2^{VS}\right)\right] \tag{55}$$

Inspection of Eq. (55) reveals that the solubility of the solute may increase in the fluid phase because the numerator depends exponen-

tially in pressure. This conclusion agrees well with the fact that a supercritical fluid has essentially a liquid-type volume and, therefore liquid-type properties at high pressures, so that its solvent capability is enhanced by increasing pressures.

Equation (55) has been extensively used for correlating the experimental solubility of solids in supercritical fluids using EOS. The prediction capabilities of such a method have been recently discussed by Wisniak *et al.* [29] who have indicated that the complex topology of high-pressure equilibrium requires assessment of the *stability of the predicted equilibrium.*

The pure component fugacity reference f_i^0 for component 1 (the solvent) may be selected as discussed in Eq. (45). Component 2, considered as a pure component, will be usually present as a solid phase at the conditions of SFE, unless it exhibits the less-common regulation phenomena (*i.e.*, depression of the fusion temperature with increasing pressure, as in the case of water). Therefore, a convenient pure-component fugacity reference for component 2 is given by Eq. (53) ($f_2^0 = f_2^S$) so that from Eq. (25) the Gibbs energy of mixing for the fluid phase is given by

$$\frac{\Delta \widetilde{G}^{fp}}{RT} = x_1 \ln \frac{x_1 \hat{\phi}_1}{\phi_1^0} + x_2 \ln \frac{x_2 \hat{\phi}_2 P}{P_2^{VS} \phi_2^{\text{sat}}} - x_2 \frac{\bar{v}^S}{RT}\left(P - P_2^{VS}\right) \tag{56}$$

for a binary mixture. In addition, considering that the solid phase is composed of a pure solute, its Gibbs energy of mixing is given by

$$\frac{\Delta \widetilde{G}^S}{RT} = \frac{\Delta \overline{G}_2}{RT}\bigg|_{(x_2 \to 1)} = \ln \frac{f_2^S}{f_2^0} = 0 \tag{57}$$

According to Eq. (57) $\Delta \widetilde{G}^S/RT$ is a single point in the $\Delta \widetilde{G}/RT$ diagram because the solid phase is pure. In contrast, Eq. (56) can be evaluated in the complete composition range. These two facts are represented in Figure 19 where A represents the $\Delta \widetilde{G}^S/RT$ point and line A–B is the equilibrium tangent.

Since the solubility of the heavy solute in the fluid phase is usually low, the $\Delta \widetilde{G}/RT$ diagram is not useful or illustrate for stability analysis. This graphical difficulty may be overcome using the criterion given by Eq. (22). In particular, zero and positive minimum values(s) of $\mathfrak{J}$ will imply stability of the test phase, the composition of which may be

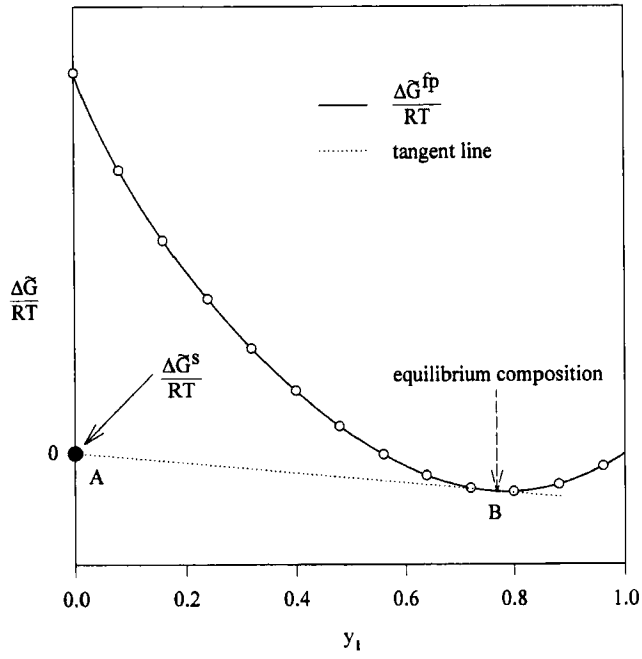

FIGURE 19 $\Delta\tilde{G}/RT$ plot for a solid–fluid equilibrium.

taken as the solubility that satisfies the necessary condition of equilibrium by Eq. (55).

Wisniak *et al.* [29] have pointed out that Eq. (55) can be readily solved for the value of the solubility using simple non-linear techniques. This situation contrasts with the complex topology of equilibrium diagrams that may occur in the neighborhood of the critical range. In order to illustrate these facts, and the potential pitfalls which may be found when predicting the solubility of heavy components in supercritical solvents, we have selected *a fictitious system* whose pure component properties are similar to those of the system carbon dioxide (1) + benzoic acid (2) (see Tab. VIII). Fugacity coefficients have been calculated by the vdW-S EOS [26] with quadratic mixing rules (Eq. (44)) and assuming a non-zero interaction parameter for the cohesion a term ($k_{ij} = -0.10$). In addition, properties have been reduced using the critical properties of the solvent (component 1 in Tab. VIII).

Figure 20 shows the solubility predicted for $T_r = 1.0026$, a temperature slightly higher than the critical temperature of the solvent, as recommended for SFE. The main features of the results are a minimum solubility at point A (the cricondenbar point, from which retrograde condensation will be observed for higher pressures), and a drastic increase of the solubility in the neighborhood of the solvent's critical point B. The latter is a consequence of the strong dependence of the fluid phase volume in the critical range. Figure 20, although a typical diagram for representing supercritical extraction data, masks of the real behavior present in critical equilibrium.

The stability of point C in Figure 20 is analyzed in Figure 21. According to the $\mathfrak{J}$ criteria, it is seen that the test composition is *not globally stable* because $\mathfrak{J}$ shows a negative minimum at point A. Such an instability is not obvious in the equilibrium diagram shown in Figure 20. A detailed map of phases may be obtained from a $P-T$

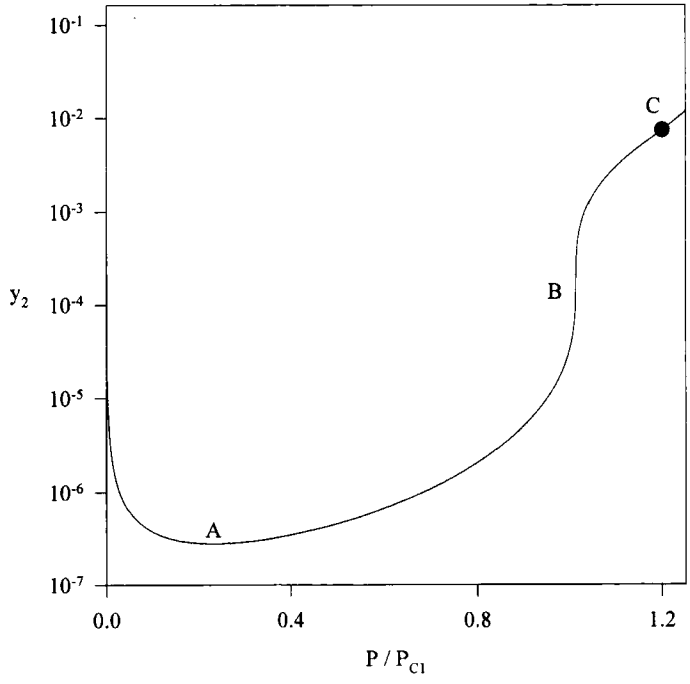

FIGURE 20 Gas solid equilibrium diagram for the mixture in Table VIII (see text for conditions and explanations).

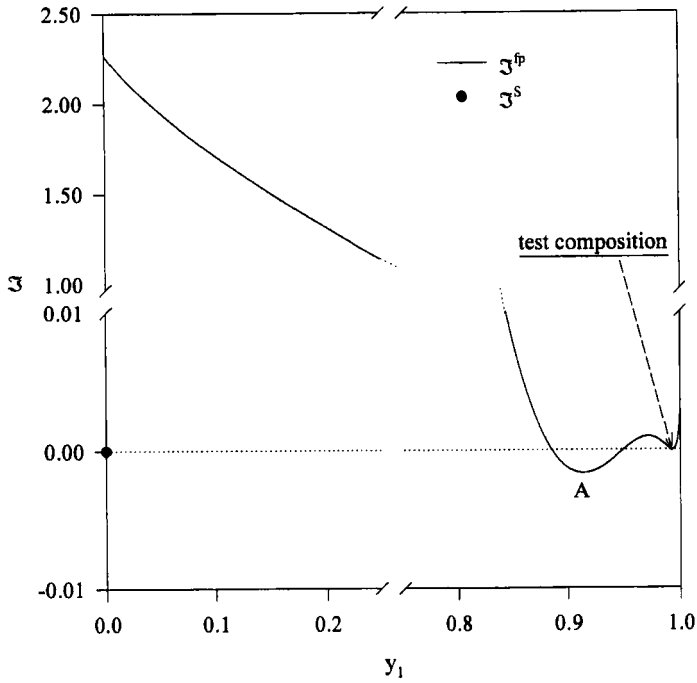

FIGURE 21 Stability analysis for point C in Figure 20.

projection of the mixture. In this diagram are represented all the equilibrium states that, according to the phase rule have one degree of freedom Figure 22a shows the $P-T$ projection generated with the vdW-S EOS, using the indicated interaction parameter and the physical properties given in Table VIII. According to Van Konynenburg and Scott [4] the mixture under consideration may be classified as Type V. However participation of solid phase incorporates a set of equilibrium states such as the gas–liquid–solid equilibrium (GLSE) and the liquid–liquid–solid equilibrium (LLSE), and an additional set of end points (LCEP's and UCEP's, lower and upper end points), consequence of the intersection of solid–fluid equilibrium states with critical lines (for further explanation see [8, 29]). Figure 22b depicts the details of Figure 22a in the neighborhood of the critical point of the solvent (component 1), where multiphase behavior becomes evident. The temperature $T_r = 1.0026$ is also indicated in Figure 22b and it is clear that it appears in a multiphase supercritical region. Starting from the low pressure range this isotherm intersects first GLSE line, then the critical gas–liquid line which joins points (1)-UCEP$_3$, after-

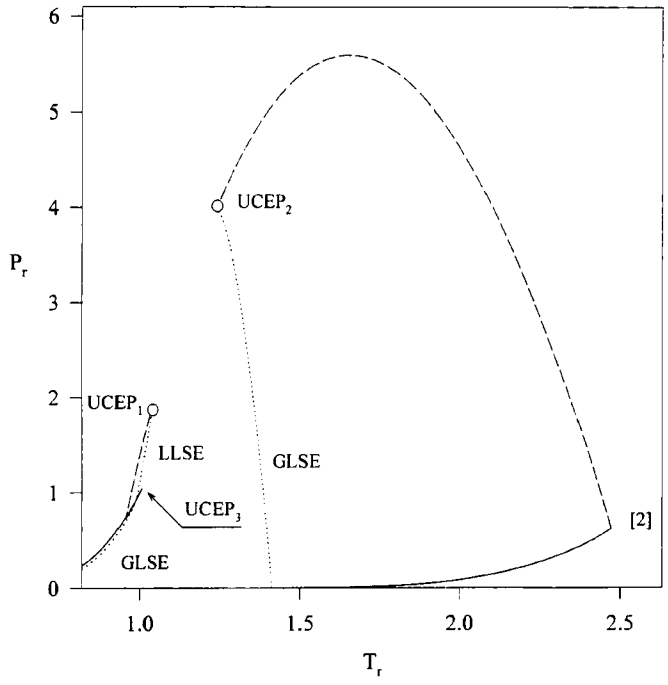

FIGURE 22a $P-T$ projection for the mixture in Table VIII.

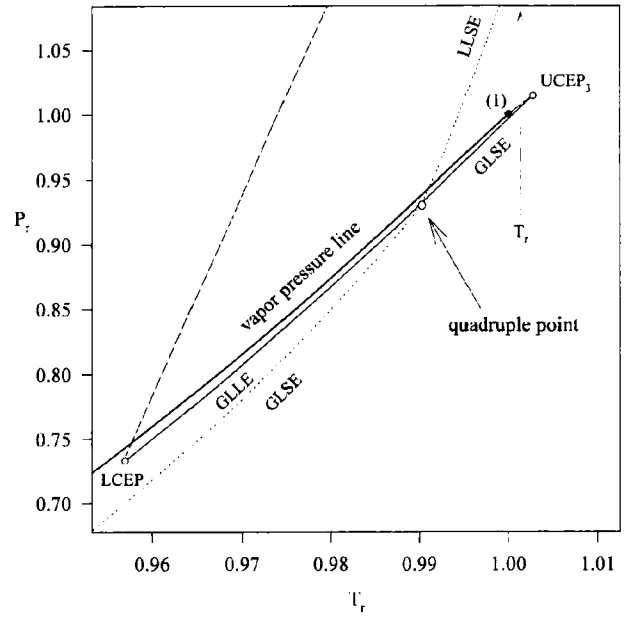

FIGURE 22b Details of Figure 22a in the neighborhood of the critical point of the solvent.

wards a LLSE line and, finally, it intersects the branch of the critical line which goes from LCEP to $UCEP_1$, giving place to a sequential evolution of phases as the pressure goes up.

A detailed inspection of the features of Figure 20 allows computation of the stable equilibrium diagram in a wide range of pressures. The stable equilibrium diagram (Fig. 23) is characterized by two three-phase lines: lines ABC and EBF which represent the GLSE and the LLSE, respectively (discussed above for the PT projection in Figs. 22). In addition, two critical points are observed (as a consequence of isotherm T_r intersecting two critical lines in Figs. 22); critical point J corresponds to a gas–liquid equilibrium (starting from the line ABC), and critical point I corresponds to a liquid–liquid equilibrium (starting from the line EFH).

Comparison of Figures 20 and 23 indicates that stability analysis plays significant role in supercritical calculations and that it should never be ignored in the treatment of experimental data.

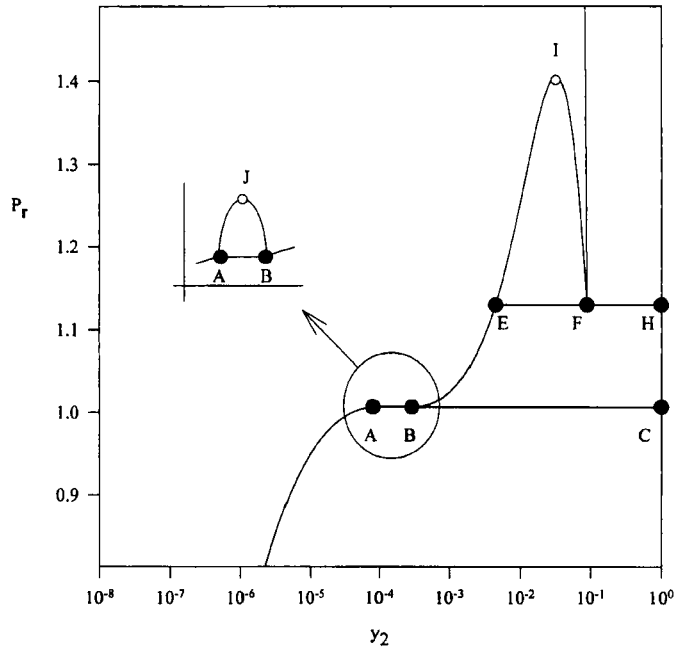

FIGURE 23 Stable equilibrium diagram for the example in Figure 20.

CONCLUSIONS

The necessary and sufficient conditions for equilibrium states require that the Gibbs energy of a thermodynamic system reach a minimum. The Gibbs energy may present multiple minima, each one representing intrinsic stability, but global stability is related only to the absolute minimum. Global stable equilibrium implies that the same equilibrium state persists independently of how a thermodynamic system is perturbed and then allowed to evolve to an equilibrium state. From a practical viewpoint, well-determined experimental phase equilibrium data are characterized by global stability *and must be modeled* under such a physical condition.

The necessary conditions of equilibrium (*i.e.*, that the Gibbs energy yields a stationary point) do not take into account the problem of phase stability, being thus *insufficient for predicting equilibrium states.* When models are taken into consideration, these necessary conditions given place to non-linear equations, like Eqs. (29), (33), (39), (51) and (55), which are routinely solved for predicting equilibrium states. However, as shown in this work, the prediction of unstable equilibrium diagrams is a potential pitfall, possibility that should be also considered. The stability of equilibrium states is a significant part of the phase equilibrium problem because it unequivocally reveals the physical validity of model predictions.

In this work we have reviewed the application of a stability analysis to common cases of binary phase equilibrium in non-electrolyte systems. Independently of the pressure range, the model, or the number of phases in equilibrium, stability analysis in binary systems allows a simple and direct graphical treatment that, in turn, is valuable of assessing data fitting or prediction by means of models. In addition, it is shown that stability analysis may be used for solving graphically complex phase equilibrium problems, allowing a rapid identification of multiphase equilibrium.

Acknowledgments

The Program of Applied Mathematics, *Fondap*, Chile, sponsored this work.

LIST OF SYMBOLS

A Helmholtz energy
a EOS cohesion parameter
b EOS covolume parameter
f fugacity
G Gibbs energy
G^E excess Gibbs energy
G_{ij} NRTL parameter
k_{ij} interaction parameter
n number of moles
P pressure
Q heat
R universal gas constant
S entropy
S_{gen} entropy generation
T temperature
U internal energy
v volume
W thermodynamic work
x, y liquid and vapor phase composition, respectively
Z compressibility factor

Greek

α_{ij} NRTL parameter
ϕ fugacity coefficient
γ activity coefficient
Δ mixing property
$\Im$ stability function defined in Eq. (21)
ψ phase fraction
τ_{ij} NRTL equation parameter
υ Poynting factor
μ chemical potential

Superscripts

A auxiliary phase
α, β pertaining to immiscible liquid phases

$*$	pertaining to a test phase or to an heteroazeotropic point
0	reference
sat	saturation property
L	pertaining to liquid phase
V	pertaining to vapor phase
S	pertaining to solid phase
fp	pertaining to fluid phase
VS	sublimation transition
R	pertaining to residual property
ig	ideal gas
$\sim$	molar property
$-$	partial property
$\wedge$	property of the component in the mixture

Subscripts

c	critical property
i,j	component index
r	reduced property

Abbreviations

EOS	pertaining to an equation of state
VLE	vapor–liquid equilibria
LLE	liquid–liquid equilibria
SLE	solid–liquid equilibria
SFE	supercritical fluid extraction
vdW	van der Waals
UCEP	upper critical end point
LCEP	lower critical end point

References

[1] Novik, J. P., Matouš, J. and Pick, J. (1987). *Liquid–Liquid Equilibria*, Elsevier, Amsterdam.
[2] Wisniak, J., Apelblat, A. and Segura, H. (1997a). *Phys. Chem. Liq.*, **35**, 1.
[3] Marcilla, A., Conesa, J. A. and Olaya, M. M. (1997). *Fluid Phase Equilibria*, **135**, 169.
[4] Van Konynenburg, P. and Scott, R. L. (1980). *Phil. Trans. R. Soc. London*, **298A**, 495–540.

[5] Edgar, T. F. and Himmelblau, D. M. (1988). *Optimization of Chemical Processes*, McGraw-Hill, Inc., pp. 138–141.
[6] Modell, M. and Reid, R. C. (1983). *Thermodynamics and its Applications*, Prentice-Hall: New Jersey.
[7] Timmermans, J. (1927). *J. Chim. Phys.*, **20**, 491.
[8] Streett, W. (1974). *Can. J. Chem. Eng.*, **52**, 92.
[9] Baker, L. E., Pierce, A. C. and Lucks, K. D. (1982). *Soc. Pet. Eng. J.*, October, 731.
[10] Michelsen, M. L. (1982). *Fluid Phase Equilibria*, **9**, 1.
[11] Sun, A. C. and Seider, W. D. (1995). *Fluid Phase Equilibria*, **103**, 213.
[12] Wasylkiewcz, S. K., Lakshmi, N. S., Doherty, M. F. and Malone, M. F. (1996). *Ind. Eng. Chem. Res.*, **35**, 1395–1408.
[13] Radzyminski, I. and Whiting, W. (1987). *Fluid Phase Equilibria*, **34**, 101.
[14] Reed, T. M. and Gubbins, K. E. (1973). *Applied Statistical Mechanics*, McGraw-Hill, New York, pp. 241–244.
[15] Van Ness, H. C. and Abbott, M. M. (1982). *Classical Thermodynamics of Non Electrolyte Solutions*, McGraw-Hill, Inc., New York.
[16] Renon, H. and Prausnitz, J. M. (1968). *AIChE J.*, **14**, 135.
[17] Guffey, C. and Wehe, A. (1972). *AIChE J.*, **18**, 913.
[18] Heidemann, R. and Mandhane, J. (1973). *Chem. Eng. Sci.*, **28**, 1213.
[19] Katayama, T., Kato, M. and Yasuda, M. (1973). *J. Chem. Eng. Japan*, **6**, 357.
[20] Mattelin, A. and Verhoeye, L. (1975). *Chem. Eng. Sci.*, **30**, 193.
[21] Wisniak, J. and Segura, H. (1997). *Ind. Eng. Chem. Res.*, **36**, 253.
[22] Gothard, F. (1981). *Ind. Eng. Chem. Fundam.*, **20**, 300.
[23] Gothard, F. (1985). *Ind. Eng. Chem. Fundam.*, **24**, 330.
[24] Syrensen, J. and Arlt, W. (1979). *Liquid–Liquid Equilibrium Data Collection. DECHEMA Chemistry Data Series*, Vol. V, 3 Parts. DECHEMA: Frankfurt.
[25] Wisniak, J., Apelblat, A. and Segura, H. (1997b). *Chem. Eng. Sci.*, **52**, 4393.
[26] Soave, G. (1984). *Chem. Engng. Sci.*, **27**, 1197.
[27] Prigogine, I. and Defay, R. (1954). *Chemical Thermodynamics*, Longmans and Green, London.
[28] Prausnitz, J. Lichtenthaler, R. and Gomes de, Azevedo (1986). E. *Molecular Thermodynamics of Fluid-Phase Equilibria.* Prentice-Hall: New Jersey.
[29] Wisniak, J., Apelblat, A. and Segura, H. (1998). *Fluid Phase Equilibria*, **147**, 45.
[30] Reid, R. C., Prausnitz, J. M. and Sherwood, T. K. (1977). *The Properties of Gases and Liquids*, McGraw-Hill, New York.
[31] Trebble, M. A. and Bishnoi, P. R. (1987). *Fluid Phase Equilibria*, **35**, 1.
[32] Patel, N. C. and Teja, A. S. (1982). *Chem. Engng. Sci.*, **37**, 463.
[33] Peng, D.-Y. and Robinson, D. B. (1976). *Ind. Eng. Chem. Fundam.*, **15**, 59.
[34] Soave, G. (1972). *Chem. Engng. Sci.*, **27**, 1197–1203.
[35] Zielke, F. and Lempe, D. A. (1997). *Fluid Phase Equilibria*, **141**, 63.
[36] Walas, S. M. (1985). *Phase Equilibria in Chemical Engineering*, Butterworth Publishers, Stoneham, MA, p. 145.

APPENDIX I

Calculation of Fugacity Coefficients Using Cubic Equations of State

A very convenient way to relate thermodynamics functions to the properties of real substances is to use cubic equations of state. Many

different forms of the EOS are reported in the literature, but the majority of them can be derived from the general cubic EOS proposed by Trebble and Bihnoi [31]

$$P = \frac{RT}{\tilde{v} - b} - \frac{a}{\tilde{v}^2 + (b - c)\tilde{v} - bc - d^2} \tag{A.I}$$

Trebble and Bishnoi indicate how parameter a, b, and c can be evaluated for each of the common EOS. All cubic EOS can be represented by the general form

$$P = \frac{RT}{\tilde{v} - b} - \frac{a}{(\tilde{v} + e_1)(\tilde{v} + e_2)} \tag{B.I}$$

For the EOS of Trebble-Bishnoi we have

$$e_1 = \frac{b + c - \sqrt{b^2 + 6cb + c^2 + 4d^2}}{2} \tag{C.1.I}$$

$$e_1 = \frac{b + c + \sqrt{b^2 + 6cb + c^2 + 4d^2}}{2} \tag{C.2.I}$$

Assuming $d = 0$ in Eq. (A.I) yields the form of the EOS of Patel and Teja [32] where e_1 and e_2 become

$$e_1 = \frac{b + c - \sqrt{b^2 + 6cb + c^2}}{2} \tag{D.1.I}$$

$$e_1 = \frac{b + c + \sqrt{b^2 + 6cb + c^2}}{2} \tag{D.2.I}$$

If, in addition, we assume that $c = b$, we get the form of the Peng and Robinson EOS [33] for which

$$e_1 = b(1 - \sqrt{2}) \tag{E.1.I}$$

$$e_1 = b(1 + \sqrt{2}) \tag{E.2.I}$$

If c is assumed to be zero we get the form of the Soave modification of Redlich-Kwong EOS [34] with

$$e_1 = 0 \tag{F.1.I}$$

$$e_1 = b \tag{F.2.I}$$

For the van der Waals EOS both e_1 and e_2 become zero.

Fugacity coefficient may be calculated for the pure compound (ϕ_i^0), for the mixture (ϕ_m), and for each of its components ($\hat{\phi}_i$). Applying Eqs. (36) and (41) to the general form of the EOS, Eq. (B.I), we get the following expression for ϕ, which is valid for calculation of ϕ_i^0 and ϕ_m:

$$\ln \phi = \frac{P\tilde{v}}{RT} - 1 - \ln \frac{P(\tilde{v} - b)}{RT} + \frac{a}{RT(e_1 - e_2)} \ln \frac{\tilde{v} + e_2}{\tilde{v} + e_1} \tag{G.I}$$

The expression for the fugacity of the component in the mixture is more complex because it depends on the number of moles of the component (composition) and thus, on the mixing rule that is used to obtain the parameters a, b, c and d. Zielke and Lempe [35] have developed the following generalized expression for $\hat{\phi}_i$ that can be applied to every cubic EOS (except van der Waals) and every mixing rule

$$\ln \hat{\phi}_i = \frac{P\tilde{v}}{RT} - 1 - \ln \frac{P(\tilde{v} - b)}{RT} + \frac{a + n\partial a/\partial n_i}{RT(e_1 - e_2)} \ln \frac{\tilde{v} + e_2}{\tilde{v} + e_1} + \frac{n\partial b/\partial n_i}{\tilde{v} - b}$$
$$+ \frac{a}{RT(e_1 - e_2)^2} \left[n \frac{\partial e_1}{\partial n_i} \left(\ln \frac{\tilde{v} + e_1}{\tilde{v} + e_2} - \frac{e_1 - e_2}{\tilde{v} + e_1} \right) \right.$$
$$\left. - n \frac{\partial e_2}{\partial n_i} \left(\ln \frac{\tilde{v} + e_1}{\tilde{v} + e_2} - \frac{e_1 - e_2}{\tilde{v} + e_2} \right) \right] \tag{H.I}$$

Equations (G.I) and (H.I) cannot be applied to the van der Waals EOS, because for it e_1 and e_1 are equal to zero. The solution for $\hat{\phi}_i$ and ϕ the van der Waals EOS can be found in the book by Walas [36].

When using Eq. (H.I) care should be taken to calculate the partial derivatives for component i assuming constant temperature, volume, and number of moles of all other component of the mixture. For ex-

ample, assuming a quadratic mixing rule for parameter a and a linear rule for all other parameters, yields the following expressions

$$n\frac{\partial a}{\partial n_i} = 2\left(\sum_k x_k a_{ik} - a\right)$$

$$n\frac{\partial b}{\partial n_i} = b_{ii} - b$$

$$n\frac{\partial e_1}{\partial n_i} = e_{1,ii} - e_1$$

$$n\frac{\partial e_2}{\partial n_i} = e_{2,ii} - e_2 \qquad \text{(I.1)}$$

A computer program written for *Mathematica* 3, for performing global stability tests using different EOS, is available from the authors.